Fracture-Cross-Flow Equilibrium in Compositional Two-Phase Reservoir Simulation

Ali Zidane, Reservoir Engineering Research Institute; and **Abbas Firoozabadi,** Reservoir Engineering Research Institute and Yale University

Summary

Compositional two-phase flow in fractured media has wide applications, including carbon dioxide (CO_2) injection in the subsurface for improved oil recovery and for CO_2 sequestration. In a recent work, we used the fracture-crossflow-equilibrium (FCFE) approach in single-phase compressible flow to simulate fractured reservoirs. In this work, we apply the same concept in compositional two-phase flow and show that we can compute all details of two-phase flow in fractured media with a central-processing-unit (CPU) time comparable with that of homogeneous media. Such a high computational efficiency is dependent on the concept of FCFE, and the implicit solution of the transport equations in the fractures to avoid the Courant-Freidricks-Levy (CFL) condition in the small fracture elements. The implicit solution of two-phase compositional flow in fractures has some challenges that do not appear in single-phase flow. The complexities arise from the upstreaming of the derivatives of the molar concentration of component i in phase $\alpha(c_{\alpha,i})$ with respect to the total molar concentration (c_i) when several fractures intersect at one interface. In addition, because of gravity, countercurrent flow may develop, which adds complexity when using the FCFE concept. We overcome these complexities by providing an upstreaming technique at the fracture/fracture interface and the matrix/fracture interface. We calculate various derivatives at constant volume V and temperature T by performing flash calculations in the fracture elements and the matrix domain to capture the discontinuity at the matrix/fracture interface. We demonstrate in various examples the efficiency and accuracy of the proposed algorithm in problems of various degrees of complexity in eight-component mixtures. In one example with 4,300 elements (1,100 fracture elements), the CPU time to 1 pore volume injection (PVI) is approximately 3 hours. Without the fractures, the CPU time is 2 hours and 28 minutes. In another example with 7,200 elements (1,200 fracture elements), the CPU time is 4 hours and 8 minutes; without fractures in homogeneous media, the CPU time is 2 hours and 53 minutes.

Introduction

Modeling of compositional two-phase flow in fractured media is of interest in CO_2 and N_2 injection, and recycling in gas–condensate reservoirs. In particular, injection of CO_2 in hydrocarbon reservoirs can reduce global warming and at the same time improve the oil recovery. To model the fracture entities, different techniques have been suggested by various authors (Bastian et al. 2000; Bogdanov et al. 2003; Geiger et al. 2004; Martin et al. 2005; Hoteit and Firoozabadi 2008; Unsal et al. 2010; Reiter et al. 2012; Zidane and Firoozabadi 2014; Abushaikhaa et al. 2015; Ahmed et al. 2015; Bahrainian and Dezfuli 2014; Chen et al. 2015; Hyman et al. 2015; Makedonska et al. 2015; Nejati et al. 2015; Andersen and Evje 2016). In this work, we will briefly review different approaches.

Original SPE manuscript received for review 19 March 2016. Revised manuscript received for review 6 September 2016. Paper (SPE 184402) peer approved 13 September 2016.

In general, the models are categorized into two broad classes: the dual-porosity/permeability models (dual-continuum) and the discrete-fracture/discrete-matrix model (DFM). Because of low computational cost, the dual-continuum models are widely used to simulate flow in fractured media (Barenblatt et al. 1960; Warren and Root 1963; Kazemi and Gilman 1969; Kazemi et al. 1992; Kazemi and Merrill 1979; Gilman and Kazemi 1983; Thomas and Thurnau 1983; Quandalle and Sabathier 1989). In the dual-continuum models, a transfer function is required to describe the exchange between the fracture network and the rock matrix. This transfer function may vary spatially in the domain. Thomas et al. (1983) presented a three-phase model to simulate flow in fractured media by use of dual porosity. An extension of the dual-porosity model by use of the multirate-transfer function was used to model incompressible two-phase flow by Di Donato et al. (2005) and Geiger et al. (2013). Transfer functions between the fractures and the rock matrix are estimated empirically (Gouze et al. 2007) and are dependent on ad-hoc shape factors. There is no theory to calculate the shape factors in two-phase flow with capillary and gravity as well as in compositional compressible flow (Hoteit and Firoozabadi 2008). In addition, in the dual-continuum models, barriers cannot be modeled. The DFM model is an alternative and is known for high accuracy and flexibility in fracture representation (Kim and Deo 2000; Karimi-Fard et al. 2004; Martin et al. 2005; Reichenberger et al. 2006; Matthäi et al. 2007a, b; Hoteit and Firoozabadi 2008; Geiger-Boschung et al. 2009; Nick and Matthäi 2011; Schmid et al. 2013; Zidane and Firoozabadi 2014; Ahmed et al. 2015). In DFM, both the matrix and the fracture entities are described explicitly in the computational domain. The fractures in DFM could have the same dimension as the matrix elements; the model is then referred to as equidimensional (Hægland et al. 2009). However, in general, fractures can be accurately modeled by a lower dimension of (n–1)-D elements **(Figs. 1a and 1b)** in an n-D domain in the DFM models (Noorishad and Mehran 1982; Baca et al. 1984; Granet et al. 1998; Ahmed et al. 2015). In a hybrid-grid method (Sandve et al. 2012), the fractures are lower-dimensional in the geometric mesh and expanded to equidimensional elements in the computational domain. In addition to making simpler mesh generation compared with the equidimensional model, the hybrid approach excludes the intermediate cell at the fracture intersections. In the equidimensional model the numerical simulation is computational-wise expensive, especially when fracture intersections are included in the problem. In addition to the previously discussed broad categories, there is a third approach that combines the dual-continuum and the DFM: the embedded-discrete-fracture model (EDFM). Li and Lee (2008) proposed the idea of EDFM and it was later adopted by Moinfar et al. (2014) and Siripatrachai et al. (2016). In this approach, there is still a need to provide the transfer function.

DFM for simulation of fractured reservoirs has received considerable attention in the last decade. Many authors have used the DFM with different discretization techniques in single-phase flow: Koudina et al. (1998) used vertex-based finite volume (FV). Caillabet et al. (2000) and Granet et al. (1998) used the cell-based control volume (CV). Martin et al. (2005) used the mixed-finite-element (FE) approximation. The FE approach was also used to model single-phase flow in fractured media (Noorishad and

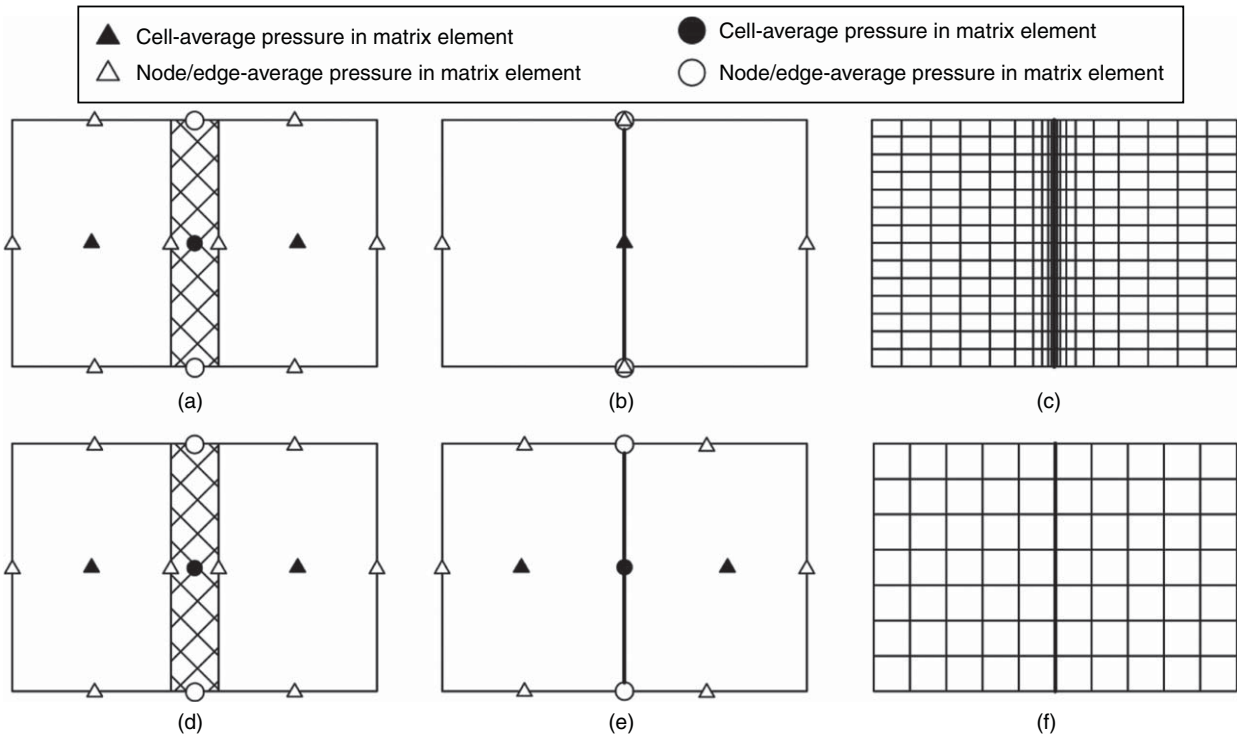

Fig. 1—Physical and computational elements in CFE (a, b, c) and in FCFE (d, e, f).

Mehran 1982; Baca et al. 1984; Juanes et al. 2002). In the context of DFM in single-phase flow, Hægland et al. (2009) used two different FV methods: a vertex-centered and cell-centered multipoint-flux approximation (MPFA). Later, Sandve et al. (2012) applied the control-volume-distributed (CVD) MPFA on a hybrid-grid method, and Ahmed et al. (2015) applied the same CVD-MPFA technique on a lower-dimensional model, both in single-phase flow. Hoteit and Firoozabadi (2005) presented the crossflow-equilibrium (CFE) concept in single-phase flow. The CFE assumes that the pressure in the fracture element is equal to the pressure in the surrounding matrix elements (Fig. 1b). This is a good assumption when the matrix elements near the fractures are sufficiently small (Fig. 1c). Zidane and Firoozabadi (2014), following the work of Martin et al. (2005), and Hoteit and Firoozabadi (2008) applied the FCFE to compressible multicomponent single-phase flow and demonstrated its efficiency to be much higher than CFE.

The DFM was extended to two-phase immiscible flow (Granet et al. 2001) by use of a cell-based CV method and a vertex-centered FV method in Reichenberger et al. (2006). Karimi-Fard et al. (2004) used the control-volume finite-difference (CVFD) method with two-point flux approximation derived from DFM in immiscible two-phase flow. To overcome the limitations of CVFD at the fracture intersections (stability and efficiency issues related to small elements at the intersection), the authors applied a transformation in these elements. The type of transformation is valid for single-phase flow but it may introduce errors in multiphase flow; the authors reported that the errors appear to be small. Nick and Matthäi (2011) used the discontinuous-finite-element/finite-volume method (DFEFVM) to model fractures in immiscible two-phase flow. DFEFVM differs from FEFVM by the extra nodes added at the matrix/fracture interfaces to capture the discontinuity in phase saturations/concentrations. DFEFVM alleviates the need to have excessive refined mesh at the fracture/matrix interfaces, which is required by FEFVM. Hoteit and Firoozabadi (2008) proposed a model for immiscible two-phase flow by use of the mixed-finite-element (MFE) and discontinuous Galerkin (DG) methods, and a lower-dimensional fracture representation in the context of FCFE with vast computational efficiency.

The DFM was also applied in compositional multiphase flow. Hoteit and Firoozabadi (2006) extended the CFE concept to compositional flow by use of the MFE and DG methods. Geiger-Boschung et al. (2009) used the FEFV method in a hybrid mesh to model multiphase compressible flow in fractured media. Hui and Mallison (2009) developed DFM on the basis of CVFD. Hui et al. (2007a, b; 2013) presented the multiple-subregion procedure to scale up the DFM to dual-porosity representation. In their model, a network of fractures is stochastically generated after specifying the distributions of fracture dimensions and orientations. In the computational model, the fractures are represented by (n–1)-D elements as interfaces of the n–D matrix elements (Lim et al. 2009; Hui et al. 2013). The multiple-subregion upscaling technique is then used to generate a coarse grid to reproduce the flow behavior of DFM.

In this work, on the basis of the concept of FCFE, we incorporate the lower-dimensional fracture model for fractures and barriers in compressible fully compositional two-phase flow with species transfer between the phases. We use the locally conservative DG method in the matrix with a FV discretization in the fractures, coupled with the mass-conservative MFE method. To avoid the CFL condition in the small fracture entities, an implicit time discretization is used in the fracture elements.

In compositional two-phase flow, the implicit solution of the transport equations is more complicated compared with single-phase flow. There are several publications on implicit formulation of the compositional two-phase flow (Fussell and Fussell 1979; Chien et al. 1985; Naimi-Tajdar et al. 2007; Voskov et al. 2009). An important aspect in compositional modeling is the choice of variables to solve for the mass-balance equations and the thermodynamic constraints. Fussell and Fussell (1979) proposed an iterative model where the variables consist of the pressure, phase densities, and mole fractions of all components. These variables are referred to as molar variables. Coats (1980) presented a fully implicit scheme for compositional multiphase flow. In his model the set of unknowns consist of pressure, saturations, and phase mole fractions. These variables are referred to as natural-type variables. Voskov et al. (2009) proposed a model where both type of variables are included (molar and natural type). Naimi-Tajdar et al. (2007) proposed a fully implicit compositional simulator derived from the generalized dual-porosity model. In their model, an iterative scheme is used to update the mass-balance equations in the domain. In our compositional two-phase flow, we use the

volume/temperature (*VT*) framework to compute coefficients of the transport equations. The variables in our model are dependent on the variation of pressure and number of moles in either gas or liquid phase with respect to overall moles of all components. This approach provides remarkable efficiency in implicit formulation (Zidane and Firoozabadi 2015).

In this work, our implicit model (Zidane and Firoozabadi 2015) is adapted in the small fracture elements to avoid the CFL condition. Solving the transport equations implicitly in the fractures and explicitly in the matrix domain makes the time scheme in our model similar to the adaptive implicit method (AIM) (Thomas and Thurnau 1983; Russell 1989; Collins et al. 1992; de Loubens et al. 2009). In the AIM, different levels of implicitness are used in adjacent gridblocks, and these levels could shift in space to maintain stability. In our model, however, the flow and transport equations are decoupled, and the phase fluxes are updated by use of the MFE (Zidane and Firoozabadi 2015), where we have demonstrated the robustness of our implicit technique compared with the existing commercial simulators. The application of our implicit model was limited to unfractured media (Zidane and Firoozabadi 2015). Compositional simulation of fractured reservoirs is more challenging because of the large range in spatial scales, permeabilities, and fluxes between the matrix domain and the fracture network. The variations of molar concentration of component i in phase $\alpha(c_{\alpha,i})$ with respect to the overall molar concentration of component i (c_i) (or $\partial c_\alpha x_{i,\alpha}/\partial c z_i$) are accounted for in our model. These derivatives are sensitive to the composition in each phase. The computation of the equilibrium compositions in all phases is provided by the equality of fugacities of each component in gas and liquid phases. This calculation is commonly referred to as flash (Firoozabadi 2015). To capture the discontinuity at the matrix/fracture interface in phase compositions and the corresponding derivatives, we perform flash calculations in both the fracture and the matrix elements, as we will discuss later.

The rest of the paper is organized as follows. In the next section we provide a general description of the model, followed by differential equations describing the multicomponent compressible two-phase flow in fractured porous media. Then we discuss the discretization of pressure and species mass-balance equations. Some of the derivations appear in Appendix A. We demonstrate the efficiency and accuracy of our model in several examples.

General Description of the Model

In our approach the total flux at the interface of the matrix and the fracture elements is calculated by the hybridized MFE method (Raviart and Thomas 1977; Brezzi and Fortin 1991; Hoteit and Firoozabadi 2005; Ackerer and Younes 2008; Younes et al. 2011, 2014; D'Angelo and Scotti 2012; Zidane et al. 2012, 2014a, b; Zidane and Firoozabadi 2014; Shahraeeni et al. 2015). In the MFE method, we evaluate the pressure inside a finite element and traces of pressure at the interfaces of each finite element in the computational domain. The phase fluxes are deduced from the total flux from the phase mobility. The discretization of the transport equations is based on the FV method in the fracture elements and higher-order DG method in the matrix elements. The DG method is known to be mass conservative at the element level and also has low numerical dispersion. When using higher-order methods, one may expect nonphysical oscillations. A multidimensional slope limiter is used to reconstruct the molar densities over the simulation domain. By using the maximum principle, the slope limiter imposes local constraints in such a way that the reconstructed molar densities in each element remain between the minimum and the maximum of the cell averages of all the surrounding elements. The MFE-DG efficiency has been demonstrated in several publications (Siegel et al. 1997; Younes et al. 2011, 2014). The higher-order methods coupled with FCFE in the DF approach can be applied to field-scale problems (in order of kilometer-long domains), as we will show in the examples.

We refer to our model as the FCFE. The CFE model proposed by Hoteit and Firoozabadi (2005) assumes the pressure in the fracture (as well as the transport variables, such as molar density and compositions) to be equal to the pressure in the adjacent matrix elements (Fig. 1b). In this approach, the matrix elements near the fractures are assumed to be small (Fig. 1c). In an implicit-pressure/explicit-concentration scheme, the CFL condition makes the CFE approach computational-wise expensive. In the FCFE model, we assume a constant pressure across the fracture width (Figs. 1d and 1e). The pressure and/or molar densities in the fracture and the adjacent matrix elements may not be the same. This alleviates the need for small elements near the fractures. The most-severe CFL condition comes from an explicit time discretization of the mass-balance equations in the small fracture elements. To overcome the CFL restriction in the fracture network, an implicit time discretization is used to compute the species-transport equations inside the fractures, as will be discussed later. This approach was adopted in Hoteit and Firoozabadi (2008) for incompressible two-phase flow and in Zidane and Firoozabadi (2014) for compressible single-phase flow. Zidane and Firoozabadi (2014) demonstrated that in single-phase flow, the CFE model converges to the same solution as FCFE only if the mesh is refined significantly so that the matrix elements near the fractures are relatively small compared with the rest of the elements. Extension from single-phase to two-phase has subtleties. When using the Newton-Raphson (NR) method in the implicit solution of compositional two-phase flow, variation of molar densities of each component in the two phases with respect to the global molar density ($\partial c_{\alpha,i}/\partial c z_i$) should be known. In single-phase flow, there is only one molar density for each component, and as a result the derivative is either zero or unity. In addition, countercurrent flow may occur in two-phase flow with gravity; the upstream value of such variation is not straightforward, as in single-phase flow. In the Mathematical Model section and in Appendix A, we will show in detail how we overcome these challenges. The phase fluxes in our approach are decoupled from the implicit update of the transport equations, and are updated at each timestep.

Fractures usually have higher permeability than the matrix domain (often orders of magnitude). Therefore, flow in the fracture network affects the phase behavior differently than in the matrix elements. A matrix element can be in liquid phase and the fracture element can be in a gas phase. The jump from one phase to another affects the implementation of FCFE because the fractures are represented by the interfaces of the matrix elements. The MFE-DG coupling helps to capture this jump, as we will discuss later.

The overall molar densities (c_i) are updated by use of FV in fracture elements and DG in matrix elements. In a previous work, we have used the MFE-FV formulation in an implicit scheme to model two-phase flow in unfractured media (Zidane and Firoozabadi 2015). The implicit solution of the transport equations in the fractures requires two different matrix inversions. One is related to updating the molar densities within the NR iterations, and the second is related to the derivatives of molar densities. The latter does not appear in single-phase flow. We will show later how we avoid the calculation of these derivatives in some fracture elements to reduce the computational cost. In Zidane and Firoozabadi (2015), the molar densities are evaluated by the FV method at the element center only. In this work the molar densities are evaluated with the DG method at the element nodes/edges in addition to the element center **(Figs. 2a and 2b).** The molar densities at the edges and traces of pressure allow capturing the discontinuity in composition and phase saturation at the matrix/fracture interface in FCFE. The overall mole fraction of all the components are calculated from the overall molar densities by use of $(z_i = c_i/c)$, where c is the molar density of the mixture. The trace of pressure, temperature, and updated overall mole fraction are used to perform flash calculations in FCFE elements to capture the discontinuity at the matrix/fracture interface in phase composition and saturation.

In the global system of equations, the pressure system is solved implicitly in both the matrix domain and the fracture network. First, traces of pressure are updated, and then pressure at the element level is evaluated through back substitution to reduce the size of the global system of equations. Once pressure and

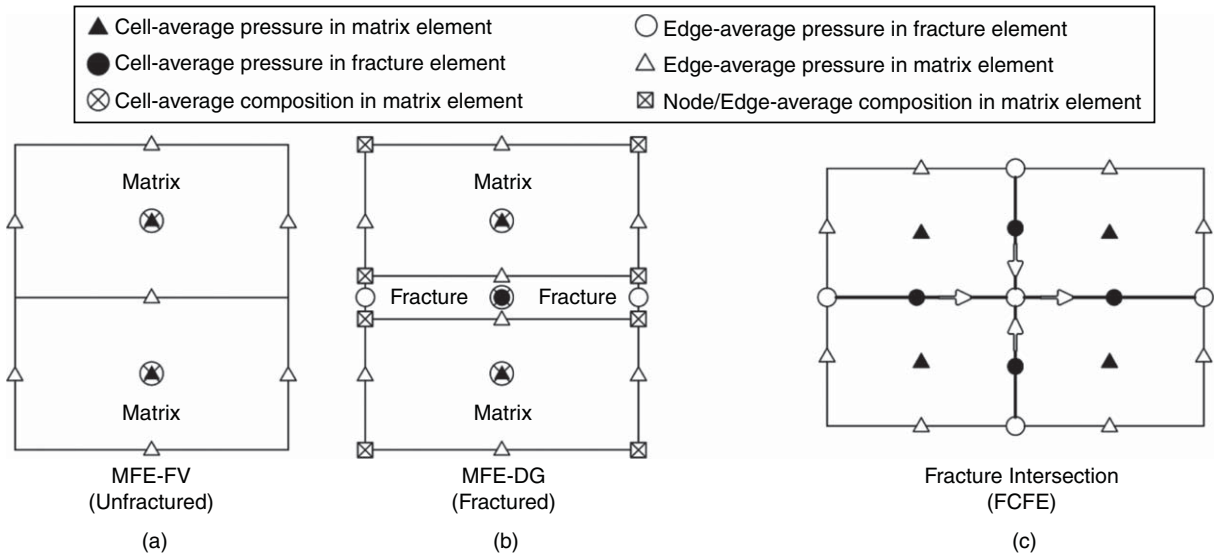

Fig. 2—Variables in unfractured domain in (a) MFE-FV, (b) fractured domain in MFE-DG, and (c) fracture intersection in FCFE.

traces of pressure are calculated, the fluxes at the interfaces are evaluated at element levels in both the matrix and the fractures. Next, an implicit update of the mass-balance equations is made by use of the NR method (often takes two to four iterations), followed by an explicit update of the mass-balance equations in the matrix domain. In this approach, the only restriction on the size of timestep arises from the CFL condition in the matrix domain. With the accuracy of higher-order DG and the FCFE concept, large-enough elements are used in the matrix domain to allow larger timesteps.

Mathematical Model

The mathematical model is presented for the sake of completeness. The discrete fractures and the matrix have different geometrical dimensions in the simulation domain, which is n-D for the matrix domain and (n–1)-D for the fracture network. We present the governing equations separately.

Governing Equations in the Matrix. The mass balance of component i in compressible two-phase (gas and oil) flow of an n_c-component mixture is given by

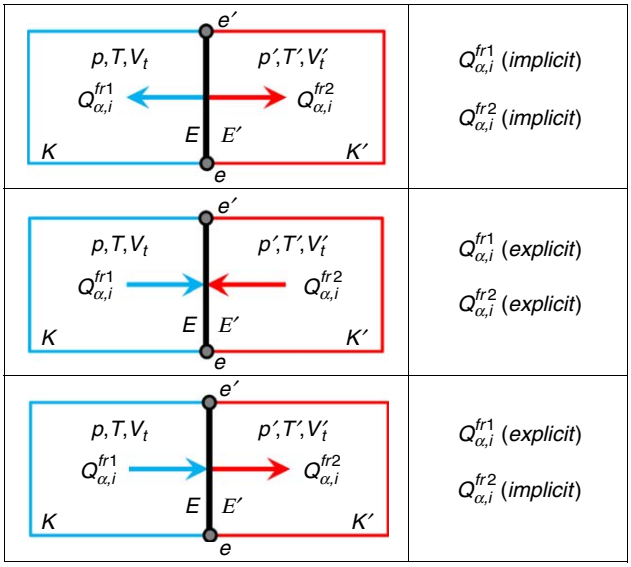

Fig. 3—Interaction between a fracture element (thick black lines) and the two adjacent matrix elements *K* and *K′*.

$$\phi\frac{\partial cz_i}{\partial t}+\nabla.\left(\sum_{\alpha}c_{\alpha}x_{i,\alpha}\boldsymbol{v}_{\alpha}\right)=F_i,\quad i=1...n_c\ \text{ in }\ \Omega\times(0,\tau),\qquad(1)$$

which is subject to the following constraints:

$$\sum_{i=1}^{n_c}z_i=\sum_{i=1}^{n_c}x_{i,\alpha}=1.\qquad(2)$$

In Eqs. 1 and 2, ϕ denotes the porosity; $\boldsymbol{v}_{\alpha}$ the velocity of phase α; c the overall molar density of the mixture; and z_i and F_i are the overall mole fraction and the sink/source term of component i in the mixture, respectively. c_{α} is the molar density of phase α and $x_{i,\alpha}$ is the mole fraction of component i in phase α. Ω is the computational domain, τ denotes the simulation time, and n_c is the number of components. We neglect diffusion in Eq. 1.

The velocity of phase α is given by Darcy's law:

$$\boldsymbol{v}_{\alpha}=-\frac{\mathbf{K}k_{r\alpha}}{\mu_{\alpha}}(\nabla p-\rho_{\alpha}\mathbf{g})=-\lambda_{\alpha}\mathbf{K}(\nabla p-\rho_{\alpha}\mathbf{g})\ ,\quad \alpha=o,g,\qquad(3)$$

where $\mathbf{K}$ is the absolute permeability; $k_{r\alpha}$, μ_{α}, and ρ_{α} are the relative permeability, dynamic viscosity, and mass density of phase α, respectively, with $\lambda_{\alpha}=k_{r\alpha}/\mu_{\alpha}$; p is the pressure; and $\mathbf{g}$ is the gravitational acceleration. The relative permeability of phase α is assumed to be a function of the phase saturation (S_{α}) by use of $k_{r\alpha}=k_{r\alpha_0}S_{\alpha}^{n}$, where $k_{r\alpha_0}$ is the endpoint relative permeability and n is a constant. A quadratic relationship is used in the matrix, and a linear relationship is used in the fractures. We use the Lohrenz-Bray-Clark model to describe the phase viscosities (Lohrenz et al. 1964). The low surface tension in compositional two-phase flow justifies the neglect of capillary pressure.

The pressure equation is derived from the concept of total volume balance (Acs et al. 1985; Watts 1986), which is given by

$$\phi C_t\frac{\partial p}{\partial t}+\sum_{i=1}^{n_c}\overline{V}_i\nabla.\left(\sum_{\alpha}c_{\alpha}x_{i,\alpha}\boldsymbol{v}_{\alpha}\right)=\sum_{i=1}^{n_c}\overline{V}_iF_i,\qquad(4)$$

where C_t is the total compressibility and $\overline{V}_i$ is the total partial molar volume of component i (Firoozabadi 2015).

The local thermodynamic equilibrium implies the equality of the fugacities of each component in the two phases:

$$f_{o,i}(T,p,x_{j,o})=f_{g,i}(T,p,x_{j,g}),\ \ i=1,...n_c\ \text{and}\ \ j=1,...n_c-1.\qquad(5)$$

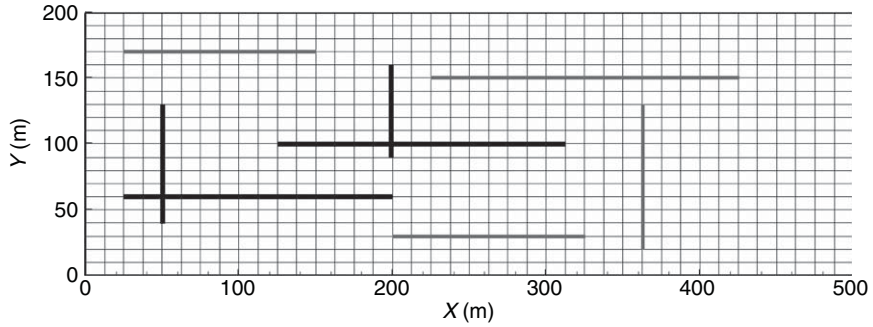

Fig. 4—Domain with fractures (thick black segments) and barriers (thin gray segments): Example 1.

In addition, we use stability analysis to incorporate the global Gibbs free-energy minimum in our calculations. The phase and volumetric behavior are described by the Peng-Robinson (PR) equation of state (EOS) (Peng and Robinson 1976):

$$c_\alpha = \frac{N_\alpha}{V_\alpha} = \frac{p}{Z_\alpha RT}, \quad \rho_\alpha = c_\alpha \sum_{i=1}^{n_c} x_{i,\alpha} M_i Z_\alpha^3 \\ -(1-B_\alpha)Z_\alpha^2 + (A_\alpha - 3B_\alpha^2 - 2B_\alpha)Z_\alpha \\ -(A_\alpha B_\alpha - B_\alpha^2 - B_\alpha^3) = 0, \quad \ldots\ldots\ldots\ldots\ldots\ldots (6)$$

where $N_\alpha, V_\alpha, Z_\alpha$ are the number of moles, volume, and compressibility factor of phase α, respectively. M_i is the molar weight of component i; R is the universal gas constant; and T is the temperature. A_α and B_α are the parameters of the PR-EOS that depend on pressure, temperature, and composition of each phase (Firoozabadi 2015).

The saturation of each phase is calculated from

$$S_\alpha = \frac{c}{c_\alpha}\omega_\alpha, \quad \ldots\ldots\ldots\ldots\ldots\ldots\ldots\ldots\ldots (7)$$

where $\omega_\alpha = N_\alpha \Big/ \sum_\beta N_\beta$, where $\beta = o, g$. From Eq. 7, the saturation constraint could be then written in the following form:

$$1 - c\left(\frac{\omega_o}{c_o} + \frac{\omega_g}{c_g}\right) = 0. \quad \ldots\ldots\ldots\ldots\ldots\ldots\ldots (8)$$

Parameter	Value
Porosity	20%
Permeability (matrix)	1 md
Permeability (fracture)	10^6 md
Fracture thickness	1 mm
Injection rate	1 PV/yr
Temperature	403.15 K
Pressure	276 bar

Table 1—Relevant data: Example 1.

Eq. 8 serves as a criterion for the selection of a timestep. The total molar densities of all the components are calculated through the mass-conservative DG method; however, the phase densities are updated by use of the EOS in phase-splitting calculations. Therefore, the total molar density from DG and phase molar densities from EOS should always follow Eq. 8 and the timestep is increased as long as Eq. 8 is satisfied and as long as the timestep is less than the matrix CFL condition. Eq. 8 cannot be relaxed, otherwise a mass-balance error is observed. The material balance in our algorithm is very low, on the order of 10^{-10}.

Governing Equations in the Fractures. In the $(n-1)$-D domain, the species mass-balance equations in the fractures are integrated along the fracture width ε:

$$\phi \frac{\partial c z_i}{\partial t} + \nabla \cdot \left[\sum_\alpha c_\alpha x_{i,\alpha} (\boldsymbol{v}_\alpha - \boldsymbol{v}_\alpha^{fr}) \right] = F_i, \quad i = 1, \ldots n_c. \\ \ldots\ldots\ldots\ldots\ldots\ldots (9)$$

We use the symbol $\boldsymbol{v}_\alpha$ for the velocity across the fracture width. For the velocity across the fracture length, we use a different symbol, $\boldsymbol{v}_\alpha^{fr}$. In the matrix we use the notation of $\boldsymbol{v}_\alpha$ as a vector to represent velocity at the interface in all faces. For the matrix face next to the fracture, $\boldsymbol{v}_\alpha = \boldsymbol{v}_\alpha^{fr}$. In the fracture element, the four velocities at the faces are represented differently. As a result, in the fracture-flow equation and in the species mass-balance equation for the fractures there are two different velocity symbols. In the discretization for the expressions for the fracture, two different velocity-exchange terms appear: one for one side of the fracture and the other from the other side of the fracture. Taken to the right-hand side of Eq. 9, this term ($\boldsymbol{v}_\alpha^{fr}$) could be treated as a sink or source term, varying with time. In the dual-porosity model, as well as in the EDFM, there is only one term that represents the exchange between the fracture element and the matrix domain. When a fracture is at the boundary of the domain, then there is one exchange term in our model.

Component	Acentric Factor	T_c (K)	p_c (bar)	Molecular Weight (g/mol)	V_c (m^3/kg)	Oil Composition (mole fraction)	Injection Gas (mole fraction)
CO_2	0.239	304.14	7.375×10^1	44	0.00214	0.0086	1
N_2	0.039	126.21	3.39×10^1	28	0.00321	0.0028	0
C_1	0.011	190.56	4.599×10^1	16	0.00615	0.4451	0
C_{2-3}	0.11783	327.81	4.654×10^1	34.96	0.00474	0.1207	0
C_{4-5}	0.21032	435.62	3.609×10^1	62.98	0.00437	0.0505	0
C_{6-10}	0.41752	574.42	2.504×10^1	110.21	0.00425	0.1328	0
C_{11-24}	0.66317	708.95	1.502×10^1	211.91	0.00443	0.1660	0
C_{25+}	1.7276	891.47	0.76×10^1	462.79	0.00417	0.0735	0

Table 2—Relevant data of oil and injected gas: Example 1.

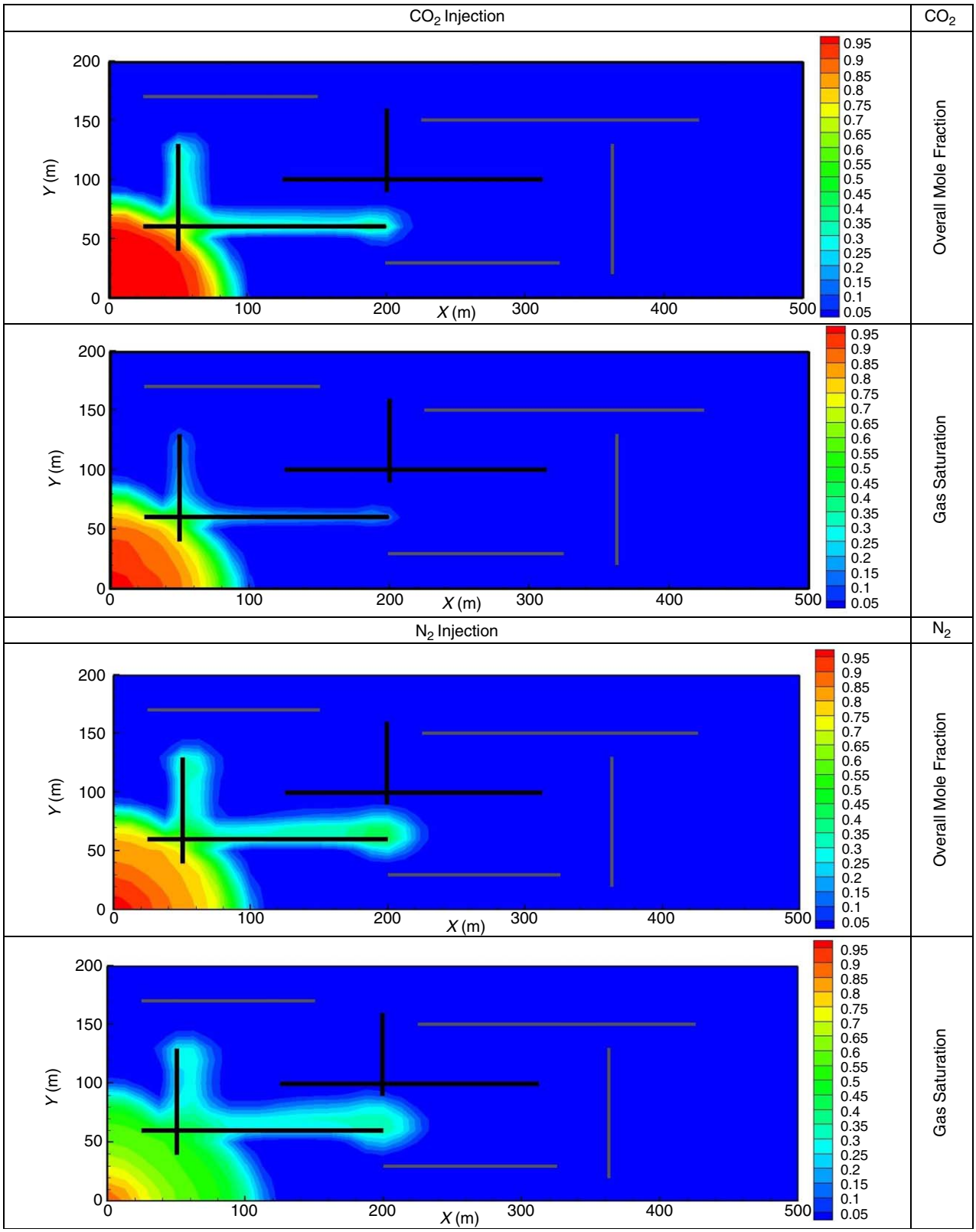

Fig. 5—Overall mole fractions of CO_2 and N_2 and gas saturation at 5% PVI: Example 1.

Similar to the pressure equation in the matrix domain, the pressure equation in the fractures is given by

$$\phi C_t \frac{\partial p}{\partial t} + \sum_{i=1}^{n_c} \overline{V}_i \left\{ \nabla \cdot \left[\sum_{\alpha} c_{\alpha} x_{i,\alpha} (\boldsymbol{v}_{\alpha} - \boldsymbol{v}_{\alpha}^{fr}) \right] - F_i \right\} = 0. \quad \cdots\cdots\cdots\cdots\cdots\cdots (10)$$

Evaluation of $\boldsymbol{v}_{\alpha}^{fr}$ will be discussed in Appendix A. The phase fluxes and viscosities in the fractures are calculated in the same manner as in the matrix domain.

Discretization

We use the DG method to discretize the species-transport equations in the matrix with a linear spatial approximation on the

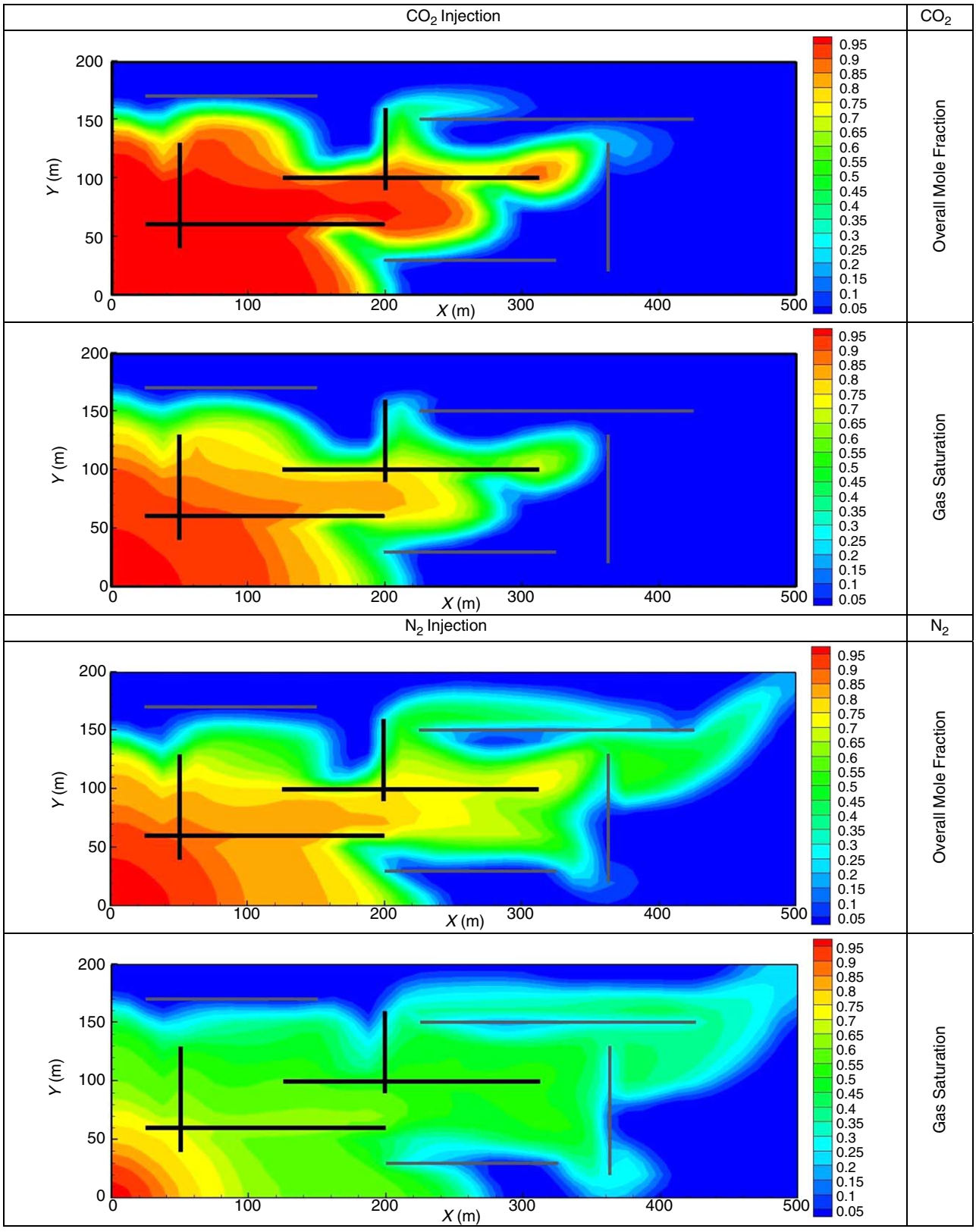

Fig. 6—Overall mole fractions of CO_2 and N_2 and gas saturation at 30% PVI: Example 1.

element level and an explicit time scheme. The transport equations in the fractures are solved implicitly by a FV discretization to reduce the computational cost. The MFE method is used to discretize the total flux in the whole domain. The lower-dimensional fractures allow more than two fracture elements intersecting at one interface (Fig. 2c). In addition, the flux between fracture elements and the matrix domain is divided into two parts, as shown in **Fig. 3.** The MFE-DG coupling provides accurate results and is efficient in CPU time in density-driven flow problems (Mosé et al. 1994; Ackerer and Younes 2008; Younes et al. 2011). Details of discretization are presented in Appendix A.

Numerical Examples

In the following, we present a set of numerical examples with eight components in structured grids to demonstrate the efficiency

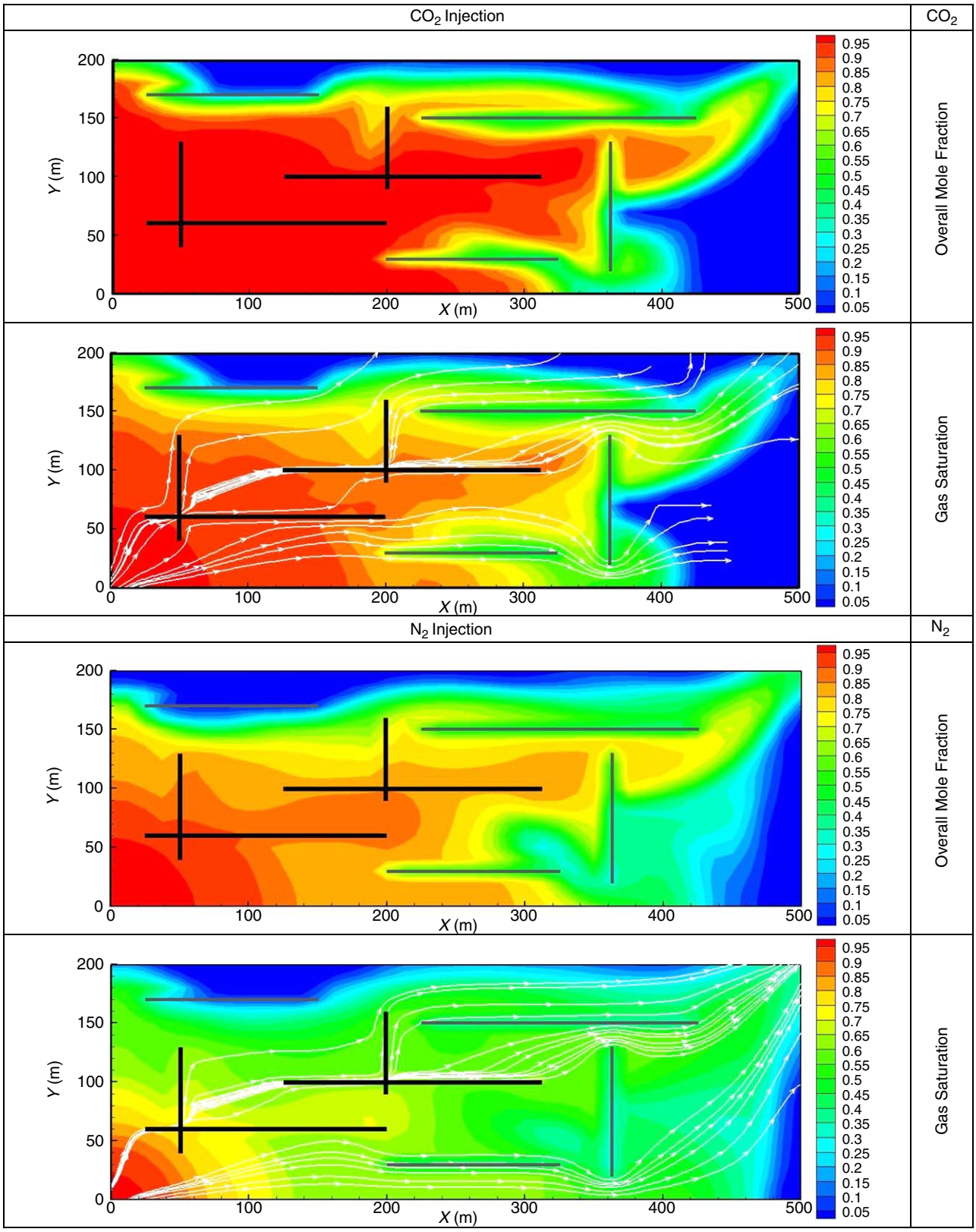

Fig. 7—Overall mole fractions of CO_2 and N_2 and gas saturation at 60% PVI (white lines represent the streamlines in gas phase): Example 1.

and accuracy of the proposed model. The use of eight components when all can dissolve in gas and liquid phases is a severe test. In compositional reservoir simulation, often four to six components can describe realistic phase behavior. An Intel Core-i5 PC with 3 GHz CPU and 4 GB of RAM is used in all the runs. Unless otherwise specified, the CPU time is given at 1 PVI.

Example 1: Fractures and Barriers. As mentioned previously, the fracture elements in FCFE are at the edges of the matrix elements. This makes the implementation of fractures and/or barriers straightforward. The barriers could be either low-permeability fractures or impermeable faults. We assume zero permeability for an impermeable fault. If an interface between

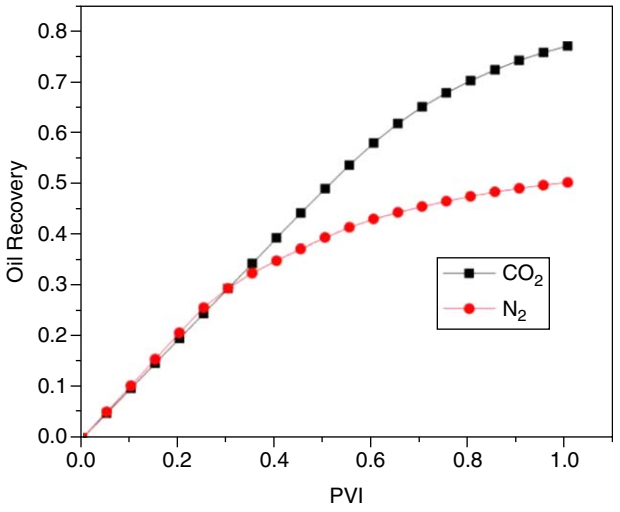

Fig. 8—Oil recovery in CO_2 and N_2 injection: Example 1.

two matrix elements is a barrier, the total and the phase fluxes are set to zero across the interface in both of the matrix elements. In this example, we consider a 500 × 200-m horizontal domain with a set of intersecting fractures and four barriers. The discretization is made by a total of 1,600 elements including 100 fracture elements. The barriers are shown by thin gray segments and the fractures by thick black segments **(Fig. 4).** The relevant data of the domain and the oil composition are given in **Tables 1 and 2,** respectively. We have examined two different cases: The first case consists of injecting N_2 into the eight-component oil, and the second case involves injecting CO_2. We use a 0.3 endpoint relative permeability for CO_2. In both cases, the gas is injected at one corner and the production well is at the opposite corner of the domain. In **Figs. 5 through 7,** we depict the overall mole fractions of CO_2 and N_2 and the gas saturation at 5, 30, and 60% PVI, respectively. The plots show that more CO_2 is dissolved into oil than N_2. N_2 breakthrough is fast. CO_2 breakthrough is approximately at 45% PVI. The recovery is enhanced by more than 25% when CO_2 is injected compared with N_2 injection **(Fig. 8).** The CPU time in this example is 1 hour and 24 minutes for CO_2 injection and 1 hour and 26 minutes for N_2 injection. In

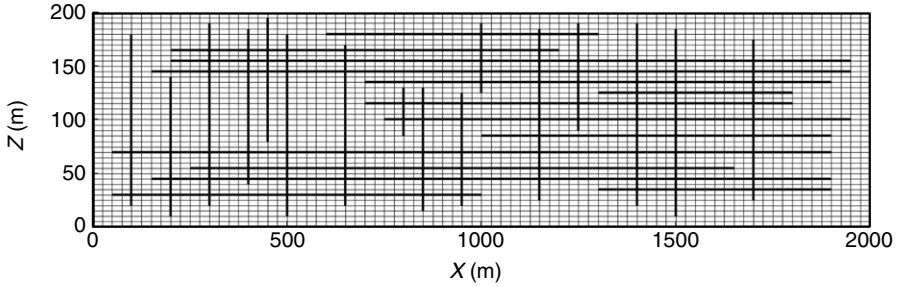

Fig. 9—Domain with fractures: Example 2.

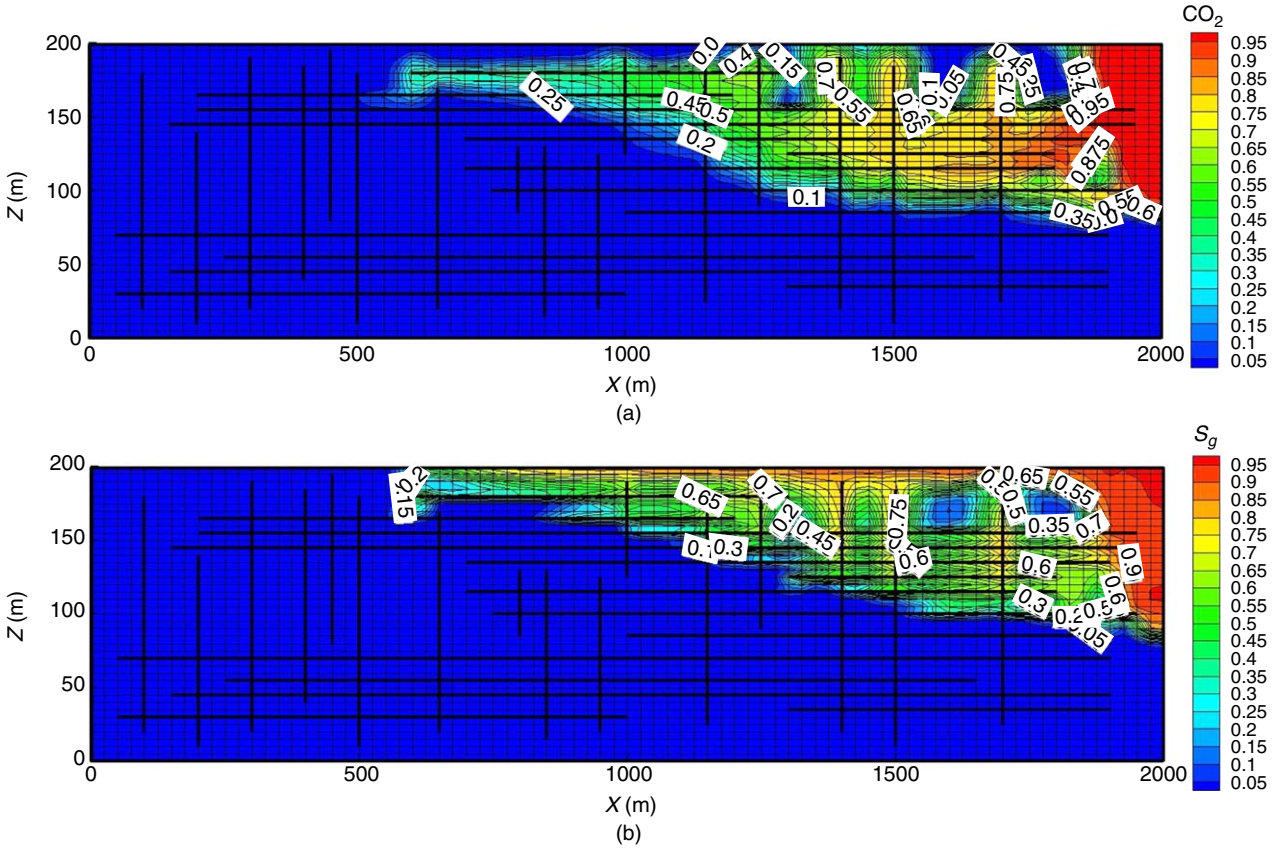

Fig. 10—(a) CO_2 overall mole fraction and (b) gas saturation at 10% PVI: Example 2.

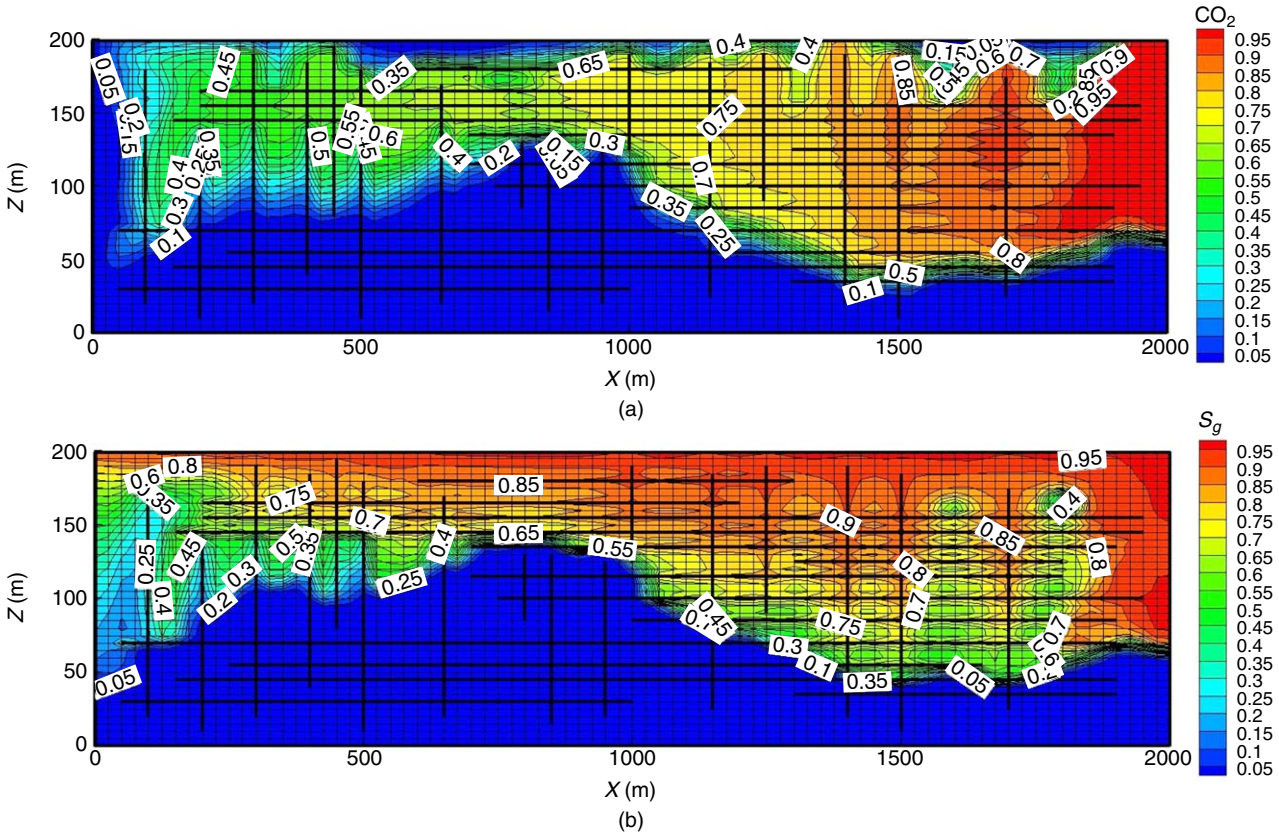

Fig. 11—(a) CO_2 overall mole fraction and (b) gas saturation at 20% PVI: Example 2.

homogeneous media, the CPU time is 51 and 52 minutes for CO_2 and N_2 injections, respectively.

Example 2: CO_2 Injection With Gravity. In this example, we consider a 2×0.2-km domain that has the same properties as the previous example. The domain with the fracture network is shown in **Fig. 9.** The numbers of matrix and fracture elements are 3,200 and 1,100, respectively. We consider the injection of CO_2 into the eight-component oil. At the reservoir conditions (276 bar at the bottom of the reservoir initially and 403 K), the mass density of CO_2 is 530 kg/m^3, which is less than the oil mass density of 660 kg/m^3. It is more efficient to inject CO_2 at the top to enhance oil recovery. CO_2 is injected at the top-right corner of the domain, and the production well is at the bottom-left corner. **Figs. 10 and 11** show the overall mole fraction of CO_2 and the gas saturation at 10 and 20% PVI, respectively. As shown in Figs. 10 and 11, because of gravity, CO_2 forms a secondary gas cap that pushes the oil down toward the production well at the bottom. Moreover, at the gas/oil interface, the light components in oil evaporate into the gas phase. The gas density therefore decreases. This effect results in the rise of gas inside the fracture network. The CPU time in this example is 3 hours and 4 minutes. In all the examples, refining the mesh does not change the results. For more details regarding the effect of mesh refinement, we present an example in Appendix B with different mesh refinements where we calculate the normalized L^2 error norm of the fluid composition at the production well. To study the effect of the fractures on CPU time in our algorithm, we have removed all the fracture elements. The CPU time of the homogeneous media is 2 hours and 28 minutes. We have also simulated the same problem in a horizontal domain, and the CPU time is 47 minutes. With gravity, countercurrent flow in a two-phase system adds complexity to flow and phase behavior. A lighter phase can rise up, which adds more restriction to the size of the timestep.

Example 3: 6-km-Long Domain. In this example, we consider a 6-km domain with 1600-m width. CO_2 is injected at one corner to displace the oil to the opposite corner. Relevant data of the problem are the same as in Example 1. The domain includes fractures that are randomly distributed **(Fig. 12).** The number of elements in the x- and y-axis are, respectively, 150 and 40, which make a total of 6,000 elements in the matrix domain. The number of fracture elements is 1,200. The overall mole fraction of CO_2 and the gas saturation at 10% PVI are shown in **Fig. 13.** The large number

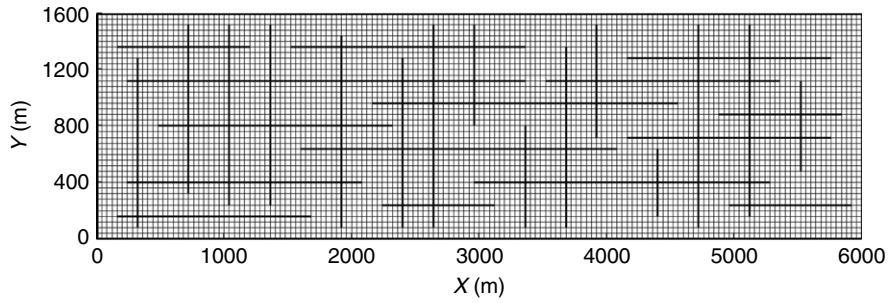

Fig. 12—Domain and mesh used, with black thick lines representing the fractures: Example 3.

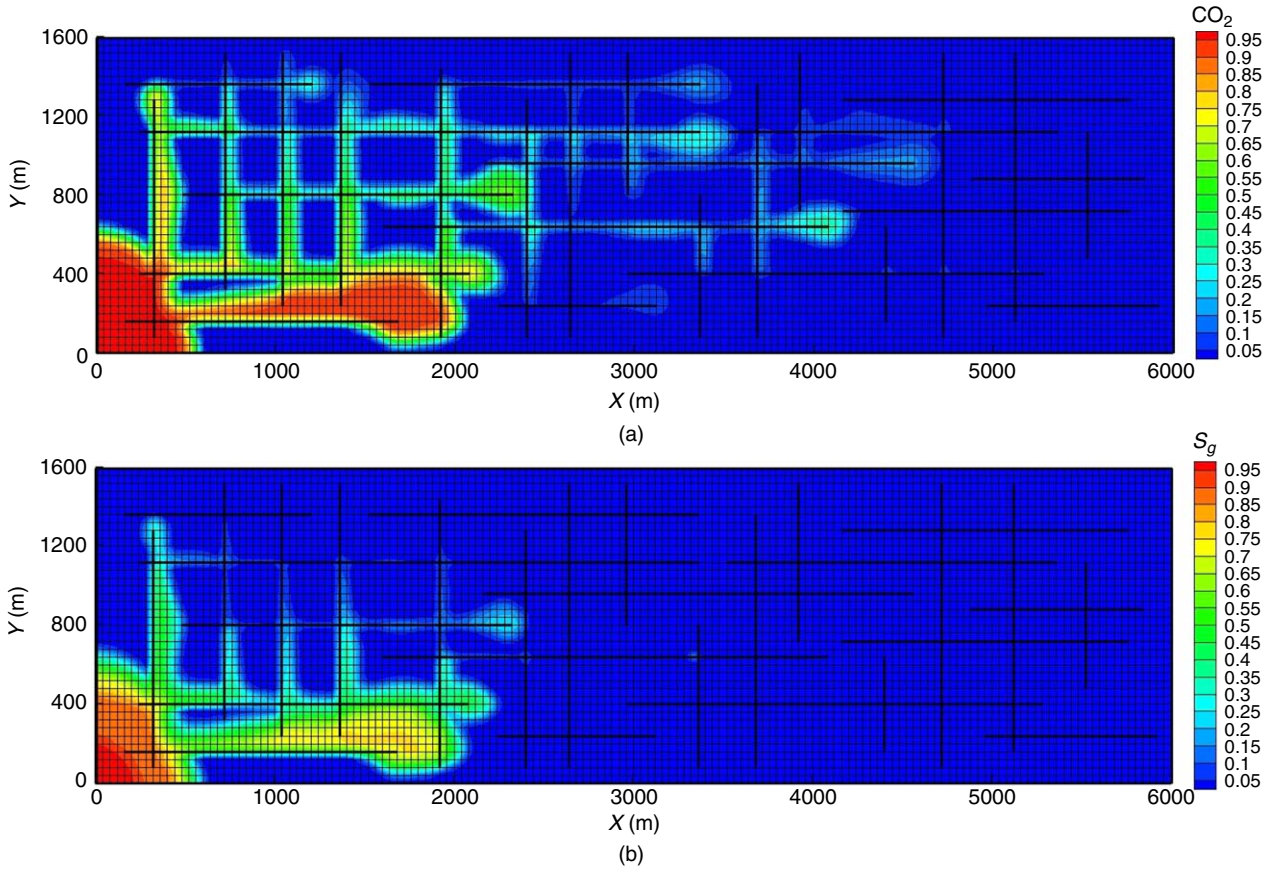

Fig. 13—(a) CO_2 overall mole fraction and (b) gas saturation at 10% PVI: Example 3.

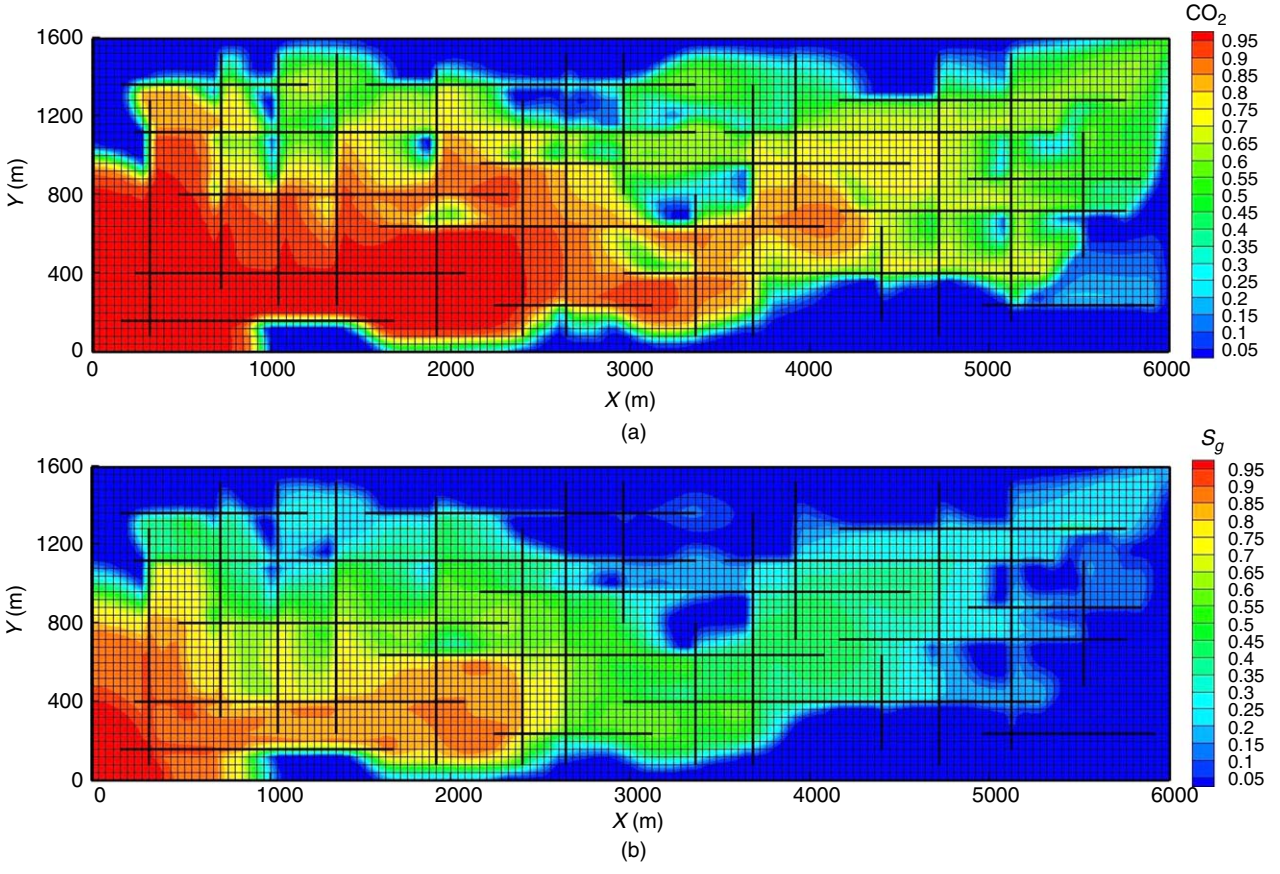

Fig. 14—(a) CO_2 overall mole fraction and (b) gas saturation at 60% PVI: Example 3.

of fracture elements in the NR iterations implies a relatively large matrix to invert. In addition, in compositional two-phase flow, the derivatives in each fracture element are updated as well, and the derivatives also require matrix inversions (Zidane and Firoozabadi 2015). However, we do not update all the derivatives for all the fractures. As seen in Fig. 13, the composition at low PVI is almost in one-third of the fractures and may be in single phase, or there may be no composition changes in two-phase. Therefore, the calculation of the derivatives is avoided in almost one-third of the fracture elements. In a similar way, at higher PVI, the fracture elements near the injection well will be saturated after some time. When these fracture elements are in single phase, then the calculation of the derivatives in these elements is also avoided. In **Fig. 14,** we show the overall mole fraction of CO_2 and the gas saturation at 60% PVI. The CPU time in this example is 4 hours and 8 minutes. The CPU time of simulating the same problem with explicit solution of the transport equation in the fractures is 46 hours and 28 minutes. Note that the high number of components affects the CPU time. The calculations carried per element are proportional to the number of components in the system. To demonstrate the efficiency of the model, we simulate the same problem by removing all the fractures; as a result, no more matrix inversions are needed in the NR method or for the calculation of the derivatives. The CPU time in unfractured homogeneous domain is 2 hours and 53 minutes. Simulation of the fractured media in our model is within the same order as in unfractured media.

Concluding Remarks

In this work, we have introduced an efficient numerical algorithm for compositional two-phase flow in fractured porous media by use of the FCFE concept, where we provide all compositions and flow paths. The main features in our model are the following.

1. Despite all details, the CPU time is comparable with that for unfractured media. The CPU time with eight-component oil in fractured media and homogeneous media differs by less than a factor of two.
2. In two-phase compositional flow, a matrix element could be in one phase and the adjacent FCFE element in a different phase. To capture the discontinuity in composition and phase saturation at the matrix/fracture interface, we perform flash calculations at the edges of the elements by use of the traces of pressure from MFE and the molar densities from DG.
3. In compositional two-phase flow, the implicit solution of the transport equation in the fractures requires two different matrix inversions. One is related to updating the molar densities within the NR iterations, and the second is related to updating the derivatives of the molar densities. The latter does not appear in single-phase flow. We avoid the calculation of these derivatives at every timestep. The derivatives of fractures in parts of the domain that are in single-phase flow (or no composition changes in two-phase flow) are not updated. This significantly reduces the size of the inverted matrix to update $\partial c_{\alpha,i}/\partial cz_i$.
4. Gravity in two-phase flow may develop countercurrent flow at the interfaces. This creates challenges related to upstreaming in multiple intersecting fractures that does not appear in single-phase flow. The upstreaming technique in our model allows calculating the derivatives to be used in NR updates when several fractures intersect at one interface.

Nomenclature

c = overall molar density
c_α = molar density
C_t = total fluid compressibility
$f_{\alpha,i}$ = fugacity
F_i = sink/source term
$\mathbf{g}$ = gravitational acceleration
g = gas
$k_{r\alpha}$ = relative permeability
$\mathbf{K}$ = absolute permeability tensor
M_i = molar weight
n_c = total number of components
N_α = number of moles
o = oil
p = pressure
Q_α^f = matrix/fracture flux
R = universal gas constant
S_α = saturation
t = time
T = temperature
$\boldsymbol{v}_\alpha$ = velocity
$\boldsymbol{v}_\alpha^{fr}$ = velocity in fractures
$\overline{V}_i$ = total partial molar volume
V_α = volume
$\boldsymbol{w}$ = Raviart-Tohmas basis vector
$x_{i,\alpha}$ = species molar fraction
z_i = overall molar fraction
Z_α = compressibility factor
α = phase index
λ_α = mobility
μ_α = viscosity
ρ_α = phase mass density
ϕ = porosity
φ = discontinuous Galerkin basis function
ω_α = phase molar fraction
Ω = computational domain

Acknowledgments

This work was supported by the member companies of the Reservoir Engineering Research Institute, whose support is gratefully acknowledged.

References

Abushaikhaa, A., Bluntb, M., Gosselinc, O. R. et al. 2015. Interface Control Volume Finite Element Method for Modelling Multi-Phase Fluid Flow in Highly Heterogeneous and Fractured Reservoirs. *J. Comput. Phys.* **298** (1 October): 41–61. https://doi.org/10.1016/j.jcp.2015.05.024.

Ackerer, P. and Younes, A. 2008. Efficient Approximations for the Simulation of Density Driven Flow in Porous Media. *Adv. Water. Resour.* **31** (1): 15–27. https://doi.org/10.1016/j.advwatres.2007.06.001.

Acs, G., Doleschall, S., and Farkas, E. 1985. General Purpose Compositional Model. *SPE J.* **25** (4): 543–553. SPE-10515-PA. https://doi.org/10.2118/10515-PA.

Ahmed, R., Edwards, M. G., Lamine, S. et al. 2015. Control-Volume Distributed Multi-Point Flux Approximation Coupled With a Lower-Dimensional Fracture Model. *J. Comput. Phys.* **284** (1 March): 462–489. https://doi.org/10.1016/j.jcp.2014.12.047.

Andersen, P.Ø. and Evje, S. 2016. A Model for Reactive Flow in Fractured Porous Media. *Chem. Eng. Sci.* **145** (12 May): 196–213. https://doi.org/10.1016/j.ces.2016.02.008.

Baca, R. G., Arnett, R. C., and Langford, D. W. 1984. Modelling Fluid Flow in Fractured-Porous Rock Masses by Finite-Element Techniques. *Int. J. Num. Meth. Fluids* **4** (4): 337–348. https://doi.org/10.1002/fld.1650040404.

Bahrainian, S. S. and Dezfuli, A. D. 2014. A Geometry-Based Adaptive Unstructured Grid Generation Algorithm for Complex Geological Media. *Comput. Geosci.* **68** (July): 31–37. https://doi.org/10.1016/j.cageo.2014.03.017.

Barenblatt, G., Zheltov, Y., and Kochina, I. 1960. Basic Concepts in the Theory of Seepage of Homogeneous Fluids in Fissurized Rocks. *J. Appl. Math. Mech.* **24** (5):1286–1303. https://doi.org/10.1016/0021-8928(60)90107-6.

Bastian, P., Chen, Z., Ewing, R. E. et al. 2000. Numerical Simulation of Multiphase Flow in Fractured Porous Media. In *Numerical Treatment of Multiphase Flows in Porous Media*, ed. Z. Chen, R. E. Ewing, and Z.-C. Shi, 50–68. Berlin: Springer-Verlag.

Bogdanov, I., Mourzenko, V., Thovert, J. et al. 2003. Two-Phase Flow Through Fractured Porous Media. *Phys. Rev. E* **68** (2): 1–24. https://doi.org/10.1103/PhysRevE.68.026703.

Brezzi, F. and Fortin, M. 1991. *Mixed and Hybrid Finite Element Methods*. New York City: Springer-Verlag.

Caillabet, Y., Fabrie, P., Landereau, P. et al. 2000. Implementation of a Finite-Volume Method for the Determination of Effective Parameters in Fissured Porous Media. *Numer. Meth. Part. D. E.* **16** (2): 237–263. https://doi.org/10.1002/(SICI)1098-2426(200003)16:2<237::AID-NUM6>3.0.CO;2-W.

Chavent, G. and Roberts, J. E. 1991. A Unified Physical Presentation of Mixed, Mixed-Hybrid Finite Element Method and Standard Finite Difference Approximations for the Determination of Velocities in Water Flow Problems. *Adv. Water Resour.* **14** (6): 329–348. https://doi.org/10.1016/0309-1708(91)90020-O.

Chavent, G., Cohen, G., Jaffre, J. et al. 1990. Discontinuous and Mixed Finite Elements for Two-Phase Incompressible Flow. *SPE Res Eng* **5** (4): 567–575. SPE-16018-PA. https://doi.org/10.2118/16018-PA.

Chen, J., Li, T., and Zhang, Y. 2015. Application of the Unstructured Grids in the Numerical Simulation of Fractured Horizontal Wells in Ultra-Low Permeability Gas Reservoirs. *J. Nat. Gas Sci. Eng.* **22** (January): 580–590. https://doi.org/10.1016/j.jngse.2015.01.003.

Chien, M. C., Lee, S. T., and Chen, W. H. 1985. A New Fully Implicit Compositional Simulator. Presented at the SPE Reservoir Simulation Symposium, Dallas, 10–13 February. SPE-13385-MS. https://doi.org/10.2118/13385-MS.

Coats, K. H. 1980. An Equation of State Compositional Model. *SPE J.* **20** (5): 363–376. SPE-8284-PA. https://doi.org/10.2118/8284-PA.

Collins, D. A., Nghiem, L. X., Li, Y.-K. et al. 1992. An Efficient Approach to Adaptive-Implicit Compositional Simulation With an Equation of State. *SPE Res Eng* **7** (2): 259–264. SPE-15133-PA. https://doi.org/10.2118/15133-PA.

D'Angelo, C. and Scotti, A. 2012. A Mixed Finite Element Method for Darcy Flow in Fractured Porous Media with Non-Matching Grids. *ESAIM-Math Model. Num.* **46** (2): 465–489. https://doi.org/10.1051/m2an/2011148.

de Loubens, R., Riaz, A., and Tchelepi, H. A. 2009. Error Analysis of an Adaptive Implicit Scheme for Hyperbolic Conservation Laws. *SIAM J. Sci. Comput.* **31** (4): 2890–2914. https://doi.org/10.1137/080724502.

Di Donato, G., Lu, H.Y., Taasoli, Z. et al. 2005. Multi-Rate Transfer Dual Porosity Modeling of Gravity Drainage Imbibition. Presented at the SPE Reservoir Simulation Symposium, The Woodlands, Texas, 31 January–2 February. SPE-93144-MS. https://doi.org/10.2118/93144-MS.

Firoozabadi, A. 2015. *Thermodynamics and Applications of Hydrocarbons Energy Production.* New York City: McGraw-Hill Education.

Fussell, L. T. and Fussell, D. D. 1979. An Iterative Technique for Compositional Reservoir Models. *SPE J.* **19** (4): 211–220. SPE-6891-PA. https://doi.org/10.2118/6891-PA.

Geiger, S., Dentz, M., and Neuweiler, I. 2013. A Novel Multi-Rate Dual-Porosity Model for Improved Simulation of Fractured and Multiporosity Reservoirs. *SPE J.* **18** (4): 670–684. SPE-148130-PA. https://doi.org/10.2118/148130-PA.

Geiger, S., Roberts, S., Matthäi, S. et al. 2004. Combining Finite Element and Finite Volume Methods for Efficient Multiphase Flow Simulations in Highly Heterogeneous and Structurally Complex Geologic Media. *Geofluids* **4** (4): 284–299. https://doi.org/10.1111/j.1468-8123.2004.00093.x.

Geiger-Boschung, S., Huangfu, Q., Reid, F. et al. 2009. Massively Parallel Sector Scale Discrete Fracture and Matrix Simulations. Presented at the SPE Reservoir Simulation Symposium, The Woodlands, Texas, 24 February. SPE-118924-MS. https://doi.org/10.2118/118924-MS.

Gilman, J. R. and Kazemi, H. 1983. Improvements in Simulation of Naturally Fractured Reservoirs. *SPE J.* **23** (4): 695–707. SPE-10511-PA. https://doi.org/10.2118/10511-PA.

Gouze, P., Borgne, L., and Leprovost, R. 2007. Non-Fickian Dispersion in Porous Media: 1. Multiscale Measurements Using Single-Well Injection Withdrawal Tracer Tests. *Water Resour. Res.* **44** (6): W06426, 15 pages. https://doi.org/10.1029/2007WR006278.

Granet, S., Fabrie, P., Lemmonier, P. et al. 1998. A Single-phase Flow Simulation of Fractured Reservoir Using a Discrete Representation of Fractures. *Proc.,* 6th European Conference on the Mathematics of Oil Recovery (ECMOR VI), Peebles, Scotland, 8–11 September. https://doi.org/10.3997/2214-4609.201406633.

Granet, S., Fabrie, P., Lemonnier, P. et al. 2001. A Two-Phase Flow Simulation of a Fractured Reservoir Using a New Fissure Element Method. *J. Pet. Sci. Eng.* **21** (1): 35–52. https://doi.org/10.1016/S0920-4105(01)00146-2.

Hægland, H., Assteerawatt, A., Dahle, H. K. et al. 2009. Comparison of Cell- and Vertex-Centered Discretization Methods for Flow in a Two-Dimensional Discrete-Fracture-Matrix System. *Adv. Water Resour.* **32** (12): 1740–1755. https://doi.org/10.1016/j.advwatres.2009.09.006.

Hoteit, H. and Firoozabadi, A. 2005. Multicomponent Fluid Flow by Discontinuous Galerkin and Mixed Methods in Unfractured and Fractured Media. *Water Resour. Res.* **41** (11): W11412, 15 pages. https://doi.org/10.1029/2005WR004339.

Hoteit, H. and Firoozabadi, A. 2006. Compositional Modeling of Discrete-Fractured Media Without Transfer Functions by the Discontinuous Galerkin and Mixed Methods. *SPE J.* **11** (3): 341352. SPE-90277-PA. https://doi.org/10.2118/90277-PA.

Hoteit, H. and Firoozabadi, A. 2008. An Efficient Model for Incompressible Two-Phase Flow in Fractured Media. *Adv. Water Resour.* **31** (6): 891–905. https://doi.org/10.1016/j.advwatres.2008.02.004.

Hui, M.-H., Gong, B., Karimi-Fard, M. et al. 2007a. Development and Application of New Computational Procedures for Modeling Miscible Gas Injection in Fractured Reservoirs. Presented at the SPE Annual Technical Conference and Exhibition, Anaheim, California, 11–14 November. SPE-109686-MS. https://doi.org/10.2118/109686-MS.

Hui, M.-H., Kamath, J., Narr, W. et al. 2007b. Realistic Modeling of Fracture Networks in a Giant Carbonate Reservoir. Presented at the International Petroleum Technology Conference, Dubai, 4–6 December. IPTC-11386-MS. https://doi.org/10.2523/IPTC-11386-MS.

Hui, M.-H., Mallison, B. T., Fyrozjaee, M. H. et al. 2013. The Upscaling of Discrete Fracture Models for Faster, Coarse-Scale Simulations of IOR and EOR Processes for Fractured Reservoirs. Presented at the SPE Annual Technical Conference and Exhibition, New Orleans, 30 September–2 October. SPE-166075-MS. https://doi.org/10.2118/166075-MS.

Hui, M.-H. and Mallison. B. T. 2009. System and Method for Predicting Fluid Flow Characteristics Within Fractured Subsurface Reservoirs. US Patent No. 20100138196 A1.

Hyman, J. D., Karra, S., Makedonska N. et al. 2015. DFNWORKS: A Discrete Fracture Network Framework for Modeling Subsurface Flow and Transport. *Comput. Geosci.* **84** (November): 10–19. https://doi.org/10.1016/j.cageo.2015.08.001.

Juanes, R., Samper, J., and Molinero, J. 2002. A General and Efficient Formulation of Fractures and Boundary Conditions in the Finite Element Method. *Int. J. Numer. Meth. Eng.* **54** (12): 1751–1774. https://doi.org/10.1002/nme.491.

Karimi-Fard, M., Durlofsky, L. J., and Aziz, K. 2004. An Efficient Discrete-Fracture Model Applicable for General-Purpose Reservoir Simulators. *SPE J.* **9** (2): 227–236. SPE-88812-PA. https://doi.org/10.2118/88812-PA.

Kazemi, H. and Gilman, J. 1969. Pressure Transient Analysis of Naturally Fractured Reservoirs with Uniform Fracture Distribution. *SPE J.* **9** (4): 451–462. SPE-2156-A. https://doi.org/10.2118/2156-A.

Kazemi, H. and Merrill, L. 1979. Numerical Simulation of Water Imbibition in Fractured Cores. *SPE J.* **19** (3): 175–182. SPE-6895-PA. https://doi.org/10.2118/6895-PA.

Kazemi, H., Gilman, J. R., and Elsharkawy, A. M. 1992. Analytical and Numerical Solution of Oil Recovery From Fractured Reservoirs With Empirical Transfer Functions. *SPE Res Eng* **7** (2): 219–227. SPE-19849-PA. https://doi.org/10.2118/19849-PA.

Kim, J. G. and Deo, M. D. 2000. Finite-Element, Discrete-Fracture Model for Multiphase Flow in Porous Media. *AIChe J.* **46** (6): 1120–1130. https://doi.org/10.1002/aic.690460604.

Koudina, N., Gonzalez Garcia, R., Thovert, J. F. et al. 1998. Permeability of Three-Dimensional Fracture Networks. *Phys. Rev. E* **57:** 4466. https://doi.org/10.1103/PhysRevE.57.4466.

Li, L. and Lee, S. H. 2008. Efficient Field-Scale Simulation of Black Oil in a Naturally Fractured Reservoir Through Discrete Fracture Networks and Homogenized Media. *SPE Res Eval & Eng* **11** (4): 750–758. SPE-103901-PA. https://doi.org/10.2118/103901-PA.

Lim, K.-T., Hui, M.-H., and Mallison, B. T. 2009. A Next-Generation Reservoir Simulator as an Enabling Technology for a Complex Discrete Fracture Modeling Workflow. Presented at the SPE Annual Technical Conference and Exhibition, New Orleans, 4–7 October. SPE-124980-MS. https://doi.org/10.2118/124980-MS.

Lohrenz, J., Bray, B. G., and Clark, C. R. 1964. Calculating Viscosities of Reservoir Fluids From Their Compositions. *J Pet Technol* **16** (10): 1171–1176. SPE-915-PA. https://doi.org/10.2118/915-PA.

Makedonska, N., Painter, S. L., Bui, Q. M. et al. 2015. Particle Tracking Approach for Transport in Three-Dimensional Discrete Fracture Networks. *Comput. Geosci.* **19** (5): 1123–1137. https://doi.org/10.1007/s10596-015-9525-4

Martin, V., Jaffre, J., and Roberts, J. E. 2005. Modeling Fractures and Barriers as Interfaces for Flow in Porous Media. *SIAM J. Sci. Comput.* **26** (5): 1667–1691. https://doi.org/10.1137/S1064827503429363.

Matthäi, S. K., Mezentsev, A., and Belayneh, M. 2007a. Finite Element - Node-Centered Finite-Volume Two-Phase-Flow Experiments With Fractured Rock Represented by Unstructured Hybrid-Element Meshes. *SPE Res Eval & Eng* **10** (6): 740–756. SPE-93341-PA. https://doi.org/10.2118/93341-PA.

Matthäi, S. K., Geiger, S., Roberts, S. G. et al. 2007b. Numerical Simulation of Multiphase Fluid Flow in Structurally Complex Reservoirs. *Geol. Soc. Lond. Spec. Pub.* **292** (1): 405–429. https://doi.org/10.1144/SP292.22.

Moinfar, A., Varavei, A., Sepehrnoori, K. et al. 2014. Development of an Efficient Embedded Discrete Fracture Model for 3D Compositional Reservoir Simulation in Fractured Reservoirs. *SPE J.* **19** (2): 289–303. SPE-154246-PA. https://doi.org/10.2118/154246-PA.

Mosé, R., Siegel, P., Ackerer, P. et al. 1994. Application of the Mixed Hybrid Finite Element Approximation in a Ground Water Flow Model: Luxury or Necessity? *Water Resour Res.* **30** (11): 3001–3012. https://doi.org/10.1029/94WR01786.

Naimi-Tajdar, R., Han, C., Sepehrnoori, K. et al. 2007. A Fully Implicit, Compositional, Parallel Simulator for IOR Processes in Fractured Reservoirs. *SPE J.* **12** (3): 367–381. SPE-100079-PA. https://doi.org/10.2118/100079-PA.

Nejati, M., Paluszny, A., and Zimmerman, R. W. 2015. On the Use of Quarter-Point Tetrahedral Finite Eements in Linear Elastic Fracture Mechanics. *Eng. Fract. Mech.* **144** (August): 194–221. https://doi.org/10.1016/j.engfracmech.2015.06.055.

Nick, H. M. and Matthäi, S. K. 2011. Comparison of Three FE-FV Numerical Schemes for Single- and Two-Phase Flow Simulation of Fractured Porous Media. *Transport Porous Med.* **90** (2): 421–444. https://doi.org/10.1007/s11242-011-9793-y.

Noorishad, J. and Mehran, M. 1982. An Upstream Finite Element Method for Solution of Transient Transport Equation in Fractured Porous Media. *Water Resour. Res.* **18** (3): 588–596. https://doi.org/10.1029/WR018i003p00588.

Peng, D. Y. and Robinson, D. B. 1976. A New Two-Constant Equation of State. *Ind. Eng. Chem. Fundamen.* **15** (1): 59–64. https://doi.org/10.1021/i160057a011.

Quandalle, P. and Sabathier, J. C. 1989. Typical Features of a Multipurpose Reservoir Simulator. *SPE Res Eng* **4** (4): 475–480. SPE-16007-PA. https://doi.org/10.2118/16007-PA.

Raviart, P. and Thomas, J. 1977. A Mixed Finite Element Method for 2nd Order Elliptic Problems. In *Mathematical Aspects of Finite Element Methods*, ed. I. Galligani and E. Magenes, 292–315. New York City: Springer-Verlag.

Reichenberger, V., Jakobs, H., Bastian, P. et al. 2006. A Mixed-Dimensional Finite Volume Method for Multiphase Flow in Fractured Porous Media. *Adv. Water Resour.* **29** (7): 1030–1036. https://doi.org/10.1016/j.advwatres.2005.09.001.

Reiter, S., Logashenko, D., Grillo, A. et al. 2012. Preparation of Grids for Simulations of Groundwater Flow in Fractured Porous Media. *Comput. Visual Sci.* **15** (4): 209–225. https://doi.org/10.1007/s00791-013-0210-7.

Riedel, S. and Nilsson, J. W. 2015. *Electric Circuits*. Pearson Education, Inc.

Russell, T. 1989. Stability Analysis and Switching Criteria for Adaptive Implicit Methods Based on the CFL Condition. Presented at the SPE Symposium on Reservoir Simulation, Houston, 6–8 February. SPE-18416-MS. https://doi.org/10.2118/18416-MS.

Sandve, T. H., Berre, I., and Nordbotten, J. M. 2012. An Efficient Multi-Point Flux Approximation Method for Discrete Fracture–Matrix Simulations. *J. Comput. Phys.* **231** (9): 3784–3800. https://doi.org/10.1016/j.jcp.2012.01.023.

Schmid, K. S., Geiger, S., and Sorbie, K. S. 2013. Higher Order FE–FV Method on Unstructured Grids for Transport and Two-Phase Flow with Variable Viscosity in Heterogeneous Porous Media. *J. Comput. Phys.* **241** (15 May): 416–444. https://doi.org/10.1016/j.jcp.2012.12.017.

Shahraeeni, E., Moortgat, J., and Firoozabadi, A. 2015. High-Resolution Finite Element Methods for 3D Simulation of Compositionally Triggered Instabilities in Porous Media. *Comput Geosci.* **19** (4): 899–920. https://doi.org/10.1007/s10596-015-9501-z.

Siegel, P., Mosé, R., Ackerer, P. et al. 1997. Solution of the Advection-Diffusion Equation Using a Combination of Discontinuous and Mixed Finite Eements. *Int. J. Numer. Meth. Fluid.* **24** (6): 595–613. https://doi.org/10.1002/(SICI)1097-0363(19970330)24:6<595::AID-FLD512>3.0.CO;2-I.

Siripatrachai, N., Ertekin, T., and Johns, R. 2016. Compositional Simulation of Discrete Fractures Incorporating the Effect of Capillary Pressure on Phase Behavior. Presented at the SPE Improved Oil Recovery Conference, Tulsa, 11–13 April. SPE-179660-MS. https://doi.org/10.2118/179660-MS.

Thomas, G. W. and Thurnau, D. H. 1983. Reservoir Simulation Using an Adaptive Implicit Method. *SPE J.* **23** (5): 759–768. SPE-10120-PA. https://doi.org/10.2118/10120-PA.

Thomas, L. K., Dixon, T. N., and Pierson, R. G. 1983. Fractured Reservoir Simulation. *SPE J.* **23** (1): 42–54. SPE-9305-PA. https://doi.org/10.2118/9305-PA.

Unsal, E., Stephan, K., Matthäi, S. K. et al. 2010. Simulation of Multiphase Flow in Fractured Reservoirs Using a Fracture-Only Model with Transfer Functions. *Comput. Geosci.* **14** (4): 527–538. https://doi.org/10.1007/s10596-009-9168-4.

Voskov, D. V., Tchelepi, H. A., and Younis, R. 2009. General Nonlinear Solution Strategies for Multiphase Multicomponent EoS Based Simulation. Presented at the SPE Reservoir Simulation Symposium, The Woodlands, Texas, 2–4 February. SPE-118996-MS. https://doi.org/10.2118/118996-MS.

Warren, J. and Root, P. 1963. The Behavior of Naturally Fractured Reservoirs. *SPE J.* **3** (3): 245–255. SPE-426-PA. https://doi.org/10.2118/426-PA.

Watts, J. W. 1986. A Compositional Formulation of the Pressure and Saturation Equations. *SPE Res Eng* **1** (3): 243–252. SPE-12244-PA. https://doi.org/10.2118/12244-PA.

Younes, A., Konz, M., Fahs, M. et al. 2011. Modelling Variable Density Flow Problems in Heterogeneous Porous Media Using the Method of Lines and Advanced Spatial Discretization Methods. *Math. Comput. Simulat.* **81** (10): 2346–2355. https://doi.org/10.1016/j.matcom.2011.02.010.

Younes, A., Markadi, A., Zidane, A. et al. 2014. A Combination of Crouzeix-Raviart, Discontinuous Galerkin and MPFA Methods for Buoyancy-Driven Flows. *Int. J. Numer. Method. H.* **24** (3): 735–759. https://doi.org/10.1108/HFF-07-2012-0156.

Zidane, A. and Firoozabadi, A. 2014. An Efficient Numerical Model for Multicomponent Compressible Flow in Fractured Porous Media. *Adv. Water Resour.* **74** (December): 127–147. https://doi.org/10.1016/j.advwatres.2014.08.010.

Zidane, A. and Firoozabadi, A. 2015. An Implicit Numerical Model for Multicomponent Compressible Two-Phase Flow in Porous Media. *Adv. Water Resour.* **85** (November): 64–78. https://doi.org/10.1016/j.advwatres.2015.09.006.

Zidane, A., Younes, A., Huggenberger, P. et al. 2012. The Henry Semianalytical Solution for Saltwater Intrusion with Reduced Dispersion. *Water Resour. Res.* **48** (6): W06533, 10 pages. https://doi.org/10.1029/2011WR011157.

Zidane, A., Zechner, E., Huggenberger, P. et al. 2014a. On the Effects of Subsurface Parameters on Evaporite Dissolution (Switzerland). *J. Contam. Hydrol.* **160** (May): 42–52. https://doi.org/10.1016/j.jconhyd.2014.02.006.

Zidane, A., Zechner, E., Huggenberger, P. et al. 2014b. Simulation of Rock Salt Dissolution and Its Impact on Land Subsidence. *Hydrol. Earth Syst. Sci.* **18** (6): 2177–2189. https://doi.org/10.5194/hess-18-2177-2014.

Appendix A—Numerical Discretization

We first present the discretization of the species-transport equations in the matrix domain and in the fracture network. We then show the discretization of the pressure equation in the whole

domain and how to couple the fractures and the matrix to solve the system of equations for pressure in the entire domain. We also present the upstreaming technique of the derivatives in multiple intersecting fractures.

Discretization of the Transport Equations in the Matrix. In two-phase compositional flow, one element could be in gas phase and the adjacent element could be in liquid phase; the MFE-DG provides accurate description of the fluids at the interface of the neighboring elements. In the MFE, once the pressure at the element interface is known, one can find pressure at the element center. The DG method provides the compositions at the element interfaces. A flash computation is performed at the interface on the basis of the pressure at the interface from MFE and the compositions from DG. This is particularly important in fractured media, to capture the discontinuity at the matrix/fracture interface. The MFE-DG describes the physics more accurately than the lower-order methods, where the upstream quantities are dependent on the center of the elements. The basic idea in DG consists of multiplying the mass-balance equation (Eq. 1) by the shape function $\varphi_{K,j}$ and integrating over each matrix element K to obtain

$$\int_K \phi \frac{\partial cz_i}{\partial t}\varphi_{K,j} + \sum_E \int_E \sum_\alpha (c_\alpha x_{i,\alpha} \boldsymbol{v}_\alpha) n_E \varphi_{K,j} - \int_K \sum_\alpha (c_\alpha x_{i,\alpha} \boldsymbol{v}_\alpha) \nabla \varphi_{K,j} = \int_K F_i \varphi_{K,j}. \quad \text{(A-1)}$$

An explicit forward Euler time discretization is used to update cz_i in each matrix finite element. In the fracture elements, the molar densities are updated implicitly. Use of different time integrations in matrix and fractures does not affect mass conservation in our model.

The local reduction of order at the matrix/fracture interface does not imply a discretization error because the values at the same interface are discontinuous at the adjacent elements (matrix/matrix or matrix/fracture).

Discretization of the Transport Equations in the Fractures. Here, we show how we solve implicitly for the species-transport equations in the fractures. We use FV integration in the species-transport equations in the fractures (Eq. 9):

$$G_{k,i} = \phi|k| \frac{cz_{i,k}^{n+1} - cz_{i,k}^{n}}{\Delta t} + \sum_\alpha \left[\sum_{e \in \partial k} (c_\alpha x_{i,\alpha}^{n+1} q_{\alpha,k,e}) - \overline{Q}_{\alpha,i}^{fr} \right] - |k| F_i = 0, \quad \text{(A-2)}$$

where $|k|$ is the surface area of the finite element k; $c_\alpha x_{i,\alpha}$ is the upstream value of $c_\alpha x_{i,\alpha}$; and $q_{\alpha,k,e}$ is the normal flux of phase α at the interface e of element k. The term $\overline{Q}_{\alpha,i}^{fr}$ represents the mass flux of component i in phase α between the fracture and the two adjacent matrix elements. $q_{\alpha,k,e}$ is the volumetric flux between the fracture k and the surrounding fractures intersecting with k at the interface e (Fig. 2). $\overline{Q}_{\alpha,i}^{fr}$ is divided into two quantities because each fracture usually has two adjacent matrix elements (Fig. 3). If a fracture is at the boundary of the domain, the mass flux between the fracture and the matrix $\overline{Q}_{\alpha,i}^{fr}$ reduces to one side, and on the opposite side $\overline{Q}_{\alpha,i}^{fr}$ is set to zero in all the equations of the fracture element.

In Eq. A-2, $G_{k,i}$ is a function of $cz_{i,k}$ and the surrounding elements of the element k. In the NR method, we evaluate the inverse of the Jacobian matrix of a system of equations that consists of $G_{k,i}$ for all fracture elements and for all components (Zidane and Firoozabadi 2015). The derivative of $G_{k,i}$, with respect to $cz_{i,k}$ ($\partial G_{k,i}/\partial cz_i^{n+1}$), may be written as follows:

$$\frac{\partial G_{k,i}}{\partial cz_i^{n+1}} = \left(\frac{\phi|k|}{\Delta t} \pm \frac{\partial c_\alpha x_{i,\alpha}}{\partial cz_i} |Q_\alpha^{fr}| \right) + \sum_{e \in \partial k} \sum_\alpha \frac{\partial c_\alpha x_{i,\alpha}^{n+1}}{\partial cz_i^{n+1}} q_{\alpha,k,e}. \quad \text{(A-3)}$$

The two major complexities in Eq. A-3 are the evaluation of the term $\partial c_\alpha x_{i,\alpha}/\partial cz_i$ and upstreaming the derivatives in multiple fracture intersections (Fig. 2). We have shown recently how to calculate analytically the derivative $\partial c_\alpha x_{i,\alpha}/\partial cz_i$ at the conditions of constant volume and temperature (Zidane and Firoozabadi 2015). We use thermodynamic equilibrium that is based on fugacity equality and constant volume at each grid-cell element in the computational domain (Zidane and Firoozabadi 2015). In the following, we discuss how to upstream a derivative if the surrounding elements are in a different phase state than the fracture element k.

In Eq. A-3, Q_α^{fr} represents the volumetric flux (note that $\overline{Q}_{\alpha,i}^{fr}$ represents the mass flux of component i between the fracture and the adjacent matrix elements). The + sign indicates an implicit treatment of $(\partial c_\alpha x_{i,\alpha}/\partial cz_i) Q_\alpha^{fr}$ and the – sign indicates an explicit treatment during the NR iterations. The exchange between a fracture and its adjacent matrix elements includes one of three possibilities: the fracture is feeding the adjacent matrix elements; the two matrix elements are feeding the fracture; or one matrix element is feeding the fracture and the fracture is feeding the other matrix element (Fig. 3). In the first case, both of the fluxes are treated implicitly (time level $n+1$); in the second case, both are treated explicitly (time level n); and in the third case, one flux is treated implicitly and the other flux is treated explicitly. In an explicit treatment, the flux is added to the residual function at each NR iteration. In an implicit treatment, the flux is added to the calculated function during the NR iteration; the same applies to the derivative $\partial c_\alpha x_{i,\alpha}/\partial cz_i$. Note that in two-phase flow, the fracture could be feeding a matrix element in the gas phase, whereas the same matrix element is feeding the fracture in the oil phase.

We denote by $c_{\alpha,e}$ molar density of phase α at the interface e. To upstream the derivatives $\partial c_{\alpha,e} x_{i,\alpha}/\partial c_i$, we use the phase flux $q_{\alpha,k,e}$ at each interface of element k, as follows:

1. If $q_{\alpha,k,e} \geq 0$, then $\partial c_\alpha x_{i,\alpha}/\partial cz_i$ is evaluated at element k.
2. If $q_{\alpha,k,e} < 0$ and only two fractures intersect at the interface e, then $\partial c_\alpha x_{i,\alpha}/\partial cz_i$ is evaluated at the adjacent element of k that we denote by k'.
3. If $q_{\alpha,k,e} < 0$ and more than two fractures intersect at the interface e, then a combination of the conservation of mass with Kirchhoff's law (Riedel and Nilsson 2015) at the interface leads to the following equation:

$$\sum_{j=1}^{n_u} q_{\alpha,k_j,e} + \sum_{j=n_u+1}^{n_t} q_{\alpha,k_j,e} = \sum_{j=1}^{n_t} q_{\alpha,k_j,e} = 0. \quad \text{(A-4)}$$

At interface e, n_t is the total number of intersecting fractures and n_u is the number of upstreaming fluxes of phase α (Fig. 2c).

The mass balance at the interface e gives

$$\sum_{j=1}^{n_u} c_{\alpha,k_j} q_{\alpha,k_j,e} = -c_{\alpha,e} \sum_{j=n_u+1}^{n_t} q_{\alpha,k_j,e}. \quad \text{(A-5)}$$

Taking the derivative of Eq. A-5 with respect to cz_i and by use of Eq. A-4,

$$\frac{\partial c_{\alpha,e}}{\partial cz_i} = \frac{\sum_{j=1}^{n_u} \frac{\partial c_{\alpha,k_j}}{\partial cz_i} q_{\alpha,k_j,e}}{\sum_{j=1}^{n_u} q_{\alpha,k_j,e}}. \quad \text{(A-6)}$$

Discretization of the Total Flux and Phase Fluxes. In the MFE method, the total velocity in each grid cell K is written in terms of the normal fluxes across each interface E of element K as follows:

$$\boldsymbol{v} = \sum_{\boldsymbol{\alpha}} \boldsymbol{v}_{\boldsymbol{\alpha}} = \sum_{E \in \partial K} q_{K,E} \boldsymbol{w}_{K,E}, \quad \text{(A-7)}$$

where $\boldsymbol{w}_{K,E}$ is the RT_0 basis function across edge E of element K and $q_{K,E}$ is the normal flux at interface E calculated through the average cell pressure of matrix element K and the trace of pressure at the interfaces of K, as follows:

$$q_{K,E} = \alpha_{K,E} p_K - \sum_{E' \in \partial K} \beta_{K,E,E'} t p_{K,E'} - \gamma_{K,E}. \quad \text{(A-8)}$$

The coefficients $\alpha_{K,E}$, $\beta_{K,E,E'}$, and $\gamma_{K,E}$ depend on the geometry of the element and the mobility. For more details about these coefficients and the MFE formulation, one may refer to Chavent and Roberts (1991), Mosé et al. (1994), Brezzi and Fortin (1991), or Chavent et al. (1990).

Once the total velocity is evaluated, we calculate the velocity of each phase independently as follows:

$$\boldsymbol{v}_\alpha = f_\alpha(\boldsymbol{v} + \boldsymbol{G}_\alpha). \quad \text{(A-9)}$$

The phase fluxes are updated by use of the solution of molar concentrations and mole fractions from the explicit DG and implicit FV calculations. To calculate the phase flux, one needs to evaluate the phase mobilities. In absence of gravity, the upstream direction is always the direction of total flux calculated through MFE. With gravity, however, no difference was observed in applying harmonic or arithmetic average at the interface (as we will show in Appendix B).

The phase mobilities are evaluated in the upstreaming element as follows (Hoteit and Firoozabadi 2006):

$$f_\alpha = \frac{\lambda_\alpha}{\sum_\beta \lambda_\beta} \text{ and } \boldsymbol{G}_\alpha = \begin{cases} \lambda_o(\rho_o - \rho_g)g, & \text{if} \quad \alpha = g \\ \lambda_g(\rho_g - \rho_o)g, & \text{if} \quad \alpha = o \end{cases}. \quad \text{(A-10)}$$

Discretization of the Pressure Equation in Matrix. From the pressure equation (Eq. 4),

$$\int_K \phi C_t \frac{\partial p}{\partial t} + \sum_{i=1}^{n_c} \overline{V}_i \left\{ \nabla \cdot \left[\sum_\alpha c_\alpha x_{i,\alpha} f_\alpha (\boldsymbol{v}_t + \boldsymbol{G}_\alpha) \right] - F_i \right\} = 0. \quad \text{(A-11)}$$

FV integration of the pressure equation over a matrix finite element K and use of the Gauss's theorem on the divergence terms are

$$\phi |K| C_t \frac{\Delta p}{\Delta t} + \sum_{i=1}^{n_c} \overline{V}_{i,K} \times \left[\sum_\alpha \sum_{E \in \partial K} \int_E c_\alpha x_{i,\alpha} f_\alpha (\boldsymbol{v} + \boldsymbol{G}_\alpha) \cdot \boldsymbol{n}_E - F_{i,K} \right] = 0. \quad \text{(A-12)}$$

By use of Eq. A-9,

$$\phi C_t |K| \frac{\Delta p}{\Delta t} + \sum_{i=1}^{n_c} \overline{V}_i \sum_E \sum_\alpha c_\alpha x_{i,\alpha} f_\alpha q_t + \sum_{i=1}^{n_c} \overline{V}_i \sum_E \int_E \sum_\alpha c_\alpha x_{i,\alpha} f_\alpha \boldsymbol{G}_\alpha \boldsymbol{n}_E - \sum_i \overline{V}_i |K| F_i = 0. \quad \text{(A-13)}$$

By use of Eq. A-8,

$$\phi C_t |K| \frac{\Delta p}{\Delta t} + \sum_{i=1}^{n_c} \overline{V}_i \sum_E (m_{i,K,E} \alpha_{K,E} p_K^{n+1} - m_{i,K,E} \sum_{E'} \beta_{K,E,E'} T p_{K,E'}^{n+1} - m_{i,K,E} \gamma_{K,E}) + \sum_{i=1}^{n_c} \overline{V}_i \sum_E \int_E \sum_\alpha c_\alpha x_{i,\alpha} f_\alpha \boldsymbol{G}_\alpha \boldsymbol{n}_E - \sum_i \overline{V}_i |K| F_i = 0. \quad \text{(A-14)}$$

with

$$m_{i,K,E} = \sum\nolimits_\alpha c_\alpha x_{i,\alpha} f_\alpha; \; \overline{V}_{K,E} = \sum\nolimits_i \overline{V}_i m_{i,K,E},$$
$$\hat{\alpha}_{K,E} = \sum\nolimits_E \overline{V}_{K,E} \alpha_{K,E}; \; \hat{\beta}_{K,E} = \sum\nolimits_E \overline{V}_{K,E} \beta_{K,E},$$
$$s_{i,K} = \sum\nolimits_\alpha c_\alpha x_{i,\alpha} f_\alpha \boldsymbol{G}_\alpha; \; \hat{s}_{i,K,E} = \int_E s_{i,K} \cdot \boldsymbol{n}_E,$$
$$\hat{\gamma}_{K,E} = \sum\nolimits_E (\overline{V}_{K,E} \gamma_{K,E} - \sum\nolimits_i \overline{V}_i \hat{s}_{i,K,E}). \quad \text{(A-15)}$$

By substitution of Eq. A-15 into Eq. A-14,

$$\left(\frac{\phi C_t |K|}{\Delta t} + \hat{\alpha}_{K,E} \right) p_K^{n+1} - \sum_E \hat{\beta}_{K,E} T p_{K,E}^{n+1} = \frac{\phi C_t |K|}{\Delta t} p_K^n + \hat{\gamma}_{K,E} + \sum_i \overline{V}_i |K| F_i. \quad \text{(A-16)}$$

Writing Eq. A-16 in matrix form results in

$$[D^m][\boldsymbol{P^m}] - [\hat{R}^{mm} \quad \hat{R}^{mf}] \begin{bmatrix} \boldsymbol{Tp^m} \\ \boldsymbol{P^f} \end{bmatrix} = G^m, \quad \text{(A-17)}$$

With

$$D^m = \frac{\phi C_t |K|}{\Delta t} + \hat{\alpha}_{K,E},$$
$$\hat{R} = \hat{\beta}_{K,E},$$
$$G^m = \frac{\phi C_t |K|}{\Delta t} p_K^n + \hat{\gamma}_{K,E} + \sum_i \overline{V}_i |K| F_i. \quad \text{(A-18)}$$

Discretization of Pressure Equation in Fractures. By use of the same FV integration of the pressure equation (Eq. 10) over a fracture element k,

$$\phi C_t |k| \frac{\Delta p}{\Delta t} + \sum_{i=1}^{n_c} \overline{V}_{i,k} \begin{bmatrix} \sum_e \int_e \sum_\alpha c_\alpha x_{i,\alpha} f_\alpha (\boldsymbol{v} + \boldsymbol{G}_\alpha) \cdot \boldsymbol{n}_e \\ - \sum_{Ei} \int_{Ei} \sum_\alpha c_\alpha x_{i,\alpha} \boldsymbol{v}_\alpha^{fr} \cdot \boldsymbol{n}_{Ei} - |k| F_i \end{bmatrix} = 0. \quad \text{(A-19)}$$

In Eq. A-19, Ei is the number of the edges in the neighboring matrix elements of the FCFE element k. The integral over the lateral length of the fracture is computed in both of the adjacent matrix elements (Fig. 3).

In a domain where the fractures are represented by (n–1)-D in an n–D domain, three different cases apply when writing the continuity of fluxes and trace of the pressure at the matrix-element interfaces.

First, if the intersection between two matrix elements is a fracture, then the following equalities apply:

$$\begin{cases} T p_{K,E}^m = T p_{K',E}^m = p_E^f \\ q_{o,K,E}^m + q_{o,K',E}^m = Q_{o,K,E}^f \\ q_{g,K,E}^m + q_{g,K',E}^m = Q_{g,K,E}^f \end{cases}, \quad \text{(A-20)}$$

where $Q_{o,K,E}^f$ and $Q_{g,K,E}^f$ are matrix–fracture volumetric flux of oil and gas phases, respectively; the fracture element is E and the adjacent matrix elements are K and K'; p_E^f is the cell average pressure of the fracture element E; and $T p_{K,E}^m$ and $T p_{K',E}^m$ are the traces of the pressure at the interface E in matrix elements K and K', respectively. Eq. A-20 shows that the pressure at the fracture element may be different from the pressure in the adjacent matrix elements; hence, the proposed model is valid whether the interface has a very-high or very-low permeability with respect to the adjacent matrix elements.

Second, if the interface E between the two matrix elements K and K' is not a fracture, then the continuity of pressure and flux imply

Matrix	Dimensions	Elements
$R^{T,m,m}$	$N_K^m \times N_E^m$	$R_{K,E}^{T,m,m} = \alpha_{K,E}^m$
$R^{T,m,f}$	$N_E^m \times N_E^m$	$R_{K,E}^{T,m,f} = \alpha_{K,E}^m$
$M^{m,m}$	$N_E^m \times N_E^m$	$M_{E,E'}^{m,m} = \sum_{E' e \partial K} \beta_{K,E,E'}^m$
$M^{m,f}$	$N_k^f \times N_k^f$	$M_{E,E'}^{m,f} = \sum_{E' e \partial K} \beta_{K,E,E'}^m$
$M^{f,f}$	$N_e^f \times N_e^f$	$M_{E,E'}^{f,f} = \sum_{E' e \partial K} \beta_{K,E,E'}^m$

Table A-1—Dimensions and elements in matrices in the pressure equation.

$$\begin{cases} Tp_{K,E}^m = Tp_{K',E}^m \\ q_{o,K,E}^m + q_{o,K',E}^m = 0 \\ q_{g,K,E}^m + q_{g,K',E}^m = 0 \end{cases}. \quad \ldots\ldots\ldots\ldots\ldots\ldots \quad (A\text{-}21)$$

Third, if the interface E is at the domain's boundary, then

$$\begin{cases} Tp_{K,E}^m = Tp_E^D \\ q_{K,E}^m = q_E^N \end{cases}, \quad \ldots\ldots\ldots\ldots\ldots\ldots\ldots\ldots \quad (A\text{-}22)$$

where Tp_E^D is a Dirichlet boundary condition and q_E^N is a Neumann boundary condition. In this work, we assume an impermeable boundary with zero flux ($q_{K,E}^m = 0$).

From Eqs. A-20 through A-22, we obtain the following system of equations that relate pressure at the center of the matrix elements ($\boldsymbol{P}^m$) and the traces of the pressure at the matrix interfaces ($\boldsymbol{Tp}^m$) to the pressure at the center of the fracture elements ($\boldsymbol{P}^f$):

$$\begin{bmatrix} R^{T,m,m} \\ R^{T,m,f} \end{bmatrix} [\boldsymbol{P}^m] - \begin{bmatrix} M^{m,m} & M^{m,f} \\ M^{f,m} & M^{f,f} \end{bmatrix} \begin{bmatrix} \boldsymbol{Tp}^m \\ \boldsymbol{P}^f \end{bmatrix} = \begin{bmatrix} 0 \\ \boldsymbol{Q}_f \end{bmatrix}. \quad \ldots\ldots\ldots\ldots\ldots\ldots \quad (A\text{-}23)$$

The (n–1)-D representation of the fractures implies that the fracture interfaces have a negligible volume compared with the size of the fractures and the domain; hence, we assume no accumulation in the fracture intersections. The continuity of fluxes and traces of the pressure at the fracture interfaces could be expressed by

$$\begin{cases} \sum_{i=1}^{n_t} q_{k_{i,e}}^f = 0 \\ Tp_{k_{i,e}}^f = Tp_e^f, \quad i = 1 \ldots n_t \end{cases}. \quad \ldots\ldots\ldots\ldots\ldots\ldots \quad (A\text{-}24)$$

On the basis of the discussed equations in all the fracture interfaces, we obtain the system of equations that relate the pressure at the fracture elements to the traces of pressures at the fracture interfaces:

$$[R^{T,f}][\boldsymbol{P}^f] - [M^f][\boldsymbol{Tp}^f] = [0]. \quad \ldots\ldots\ldots\ldots\ldots\ldots \quad (A\text{-}25)$$

The FV integration of the pressure equation over all the fracture elements provides

$$[D^f][\boldsymbol{P}^f] - [\hat{R}^f][\boldsymbol{Tp}^f] = [\boldsymbol{G}^f + \boldsymbol{Q}_f]. \quad \ldots\ldots\ldots\ldots\ldots\ldots \quad (A\text{-}26)$$

In Eq. A-26, the term $\boldsymbol{Q}_f$ represents the total volumetric flux of gas and liquid phases of each fracture element with the adjacent matrix elements. To reduce the computational cost in our calculations, we perform the following steps.

First, we eliminate the matrix/fracture flux by subtracting Eq. A-26 from the second equation in Eq. A-23.

Next, to avoid the inversion of a large matrix at each timestep, which could be costly, we use Eq. A-17 to find the expression of $\boldsymbol{P}^m$ as a function of $\boldsymbol{Tp}^m$ and $\boldsymbol{P}^f$, as follows:

$$\boldsymbol{P}^m = [D^m]^{-1}[\boldsymbol{G}^m + \hat{R}^{mm}\boldsymbol{Tp}^m + \hat{R}^{mf}\boldsymbol{P}^f]. \quad \ldots\ldots\ldots\ldots\ldots\ldots \quad (A\text{-}27)$$

Global System of Pressure Equations. The global system of equations for pressure is dependent on the continuity of the fluxes and traces of the pressure at the interfaces of matrix elements and the fracture elements separately. After writing the continuity equations at the matrix and fracture interfaces and the volume-balance equations in matrix and fracture elements, we obtain the following global system of equations:

$$\begin{bmatrix} A^{m,m} & A^{m,f} & 0 \\ A^{f,m} & A^{f,f} & -\hat{R}^f \\ 0 & R^{T,f} & M^f \end{bmatrix} \begin{bmatrix} \boldsymbol{Tp}^m \\ \boldsymbol{P}^f \\ \boldsymbol{Tp}^f \end{bmatrix} = \begin{bmatrix} \boldsymbol{V}^m \\ \boldsymbol{V}^f \\ 0 \end{bmatrix}. \quad \ldots\ldots \quad (A\text{-}28)$$

As shown, the global system of equations relates the traces of pressure in the matrix elements to pressure and traces of the pressure in the fracture elements. The dimensions and the elements of matrices that appear in the above equations are shown in **Table A-1.**

The matrices in Eq. A-28 are therefore

$$A^{m,m} = R^{T,m,m}D^{m-1}\hat{R}^{mm} - M^{m,m}; \quad \ldots\ldots\ldots\ldots \quad (A\text{-}29a)$$

$$A^{m,f} = R^{T,m,m}D^{m-1}\hat{R}^{mf} - M^{m,f}; \quad \ldots\ldots\ldots\ldots \quad (A\text{-}29b)$$

$$A^{f,m} = -R^{T,m,f}D^{m-1}\hat{R}^{mm} + M^{f,m}; \quad \ldots\ldots\ldots\ldots \quad (A\text{-}29c)$$

$$A^{f,f} = -R^{Tm,f}D^{m-1}\hat{R}^{mf} + M^{f,f} + D^f; \quad \ldots\ldots\ldots\ldots \quad (A\text{-}29d)$$

$$V^m = -R^{T,m,f}D^{m-1}G^m; \quad \ldots\ldots\ldots\ldots\ldots\ldots \quad (A\text{-}29e)$$

$$V^f = G^f + R^{T,m,f}D^{m-1}G^m. \quad \ldots\ldots\ldots\ldots\ldots\ldots \quad (A\text{-}29f)$$

Appendix B—Convergence Tests

Example B-1 and Effect of Mesh-Refinement and Upstreaming Techniques. In this example, we study the effect of mesh refinement and the upstreaming techniques. The normalized L^2 error norm is used as a measure of accuracy.

We conduct this study in a vertical domain of 500×200 m with two horizontal fractures that are each 300 m long, and one fracture loop at the middle of the domain **(Fig. B-1).**

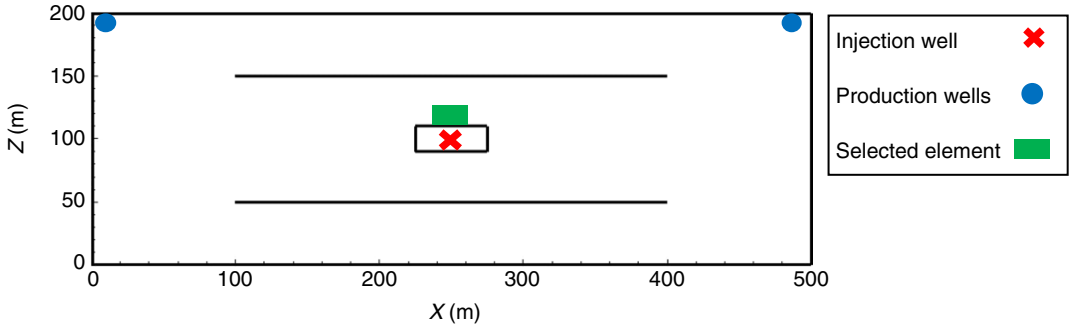

Fig. B-1—Domain and wells: Example B-1.

Parameter	Value
Porosity	20%
Permeability (matrix)	1 md
Permeability (fracture)	10^5 md
Fracture thickness	1 mm
Injection rate	0.1 PV/yr
Temperature	311 K
Initial pressure at the bottom of the domain	69 bar
Injected fluid: C_1	1 (mole fraction)
Initial fluid in the domain: C_3	1 (mole fraction)

Table B-1—Relevant data: Example B-1.

We consider injection of methane into the propane-saturated domain **(Table B-1).** The injection well is inside the fracture loop, and two production wells are at the top left and right corners of the domain (Fig. B-1). The injector inside the fracture loop in a vertical domain is a challenging example for models that use an explicit time discretization of the mass-balance equation.

To study the effect of mesh refinement on accuracy, we calculate the normalized L^2 error norm in overall mole fraction of methane at the production wells in three different meshes: Mesh-1 of 400 elements, Mesh-2 of 800 elements, and Mesh-3 of 1,600 elements **(Fig. B-2).** A more-refined mesh of 10,000 elements is used as a reference solution. As shown in **Fig. B-3,** the highest error for the coarse mesh is slightly less than 6% and shows a decreasing trend to less than 1% at the end of the simulation. In the 800 mesh, the error is always less than 4% and decreases to less than 0.5% at the end of the simulation. In the 1,600 mesh, the highest error is less than 1%. Note that methane reaches the production wells at approximately 0.38 PVI; the error is zero before breakthrough. We show the overall mole fraction of methane at 10% PVI in **Fig. B-4,** and the gas saturation at 80% PVI in **Fig. B-5.** Results in overall mole fraction and gas saturation are comparable for all meshes at low and high PVI.

In addition to effect of mesh refinement, we study the effect of mobility calculated from arithmetic and harmonic averages. The upstream mobility of a phase in one fracture element affects the phase saturation on its adjacent matrix elements. We investigate the gas saturation in the nearest matrix element on top of the horizontal-fracture element shown in Fig. B-1. The normalized L^2 error norm of gas saturation in this element is computed by use of the two upstreaming techniques: the harmonic average and the arithmetic average at different mesh refinements. The equidimensional model with 10,000 elements is used as reference solution. As shown in **Fig. B-6,** both techniques give an error of less than 0.4% and decrease to less than 0.05% with refinement.

Example B-2: Convergence Test. In this example, we perform a convergence test in a domain with a single fracture (Hægland et al. 2009; Sandve et al. 2012; Ahmed et al. 2015). A square domain of unit surface area containing a single fracture of aperture a is shown in **Fig. B-7.** We set the matrix permeability to 1 md and study three different fracture permeabilities: k_f of 10^{-4}, 1, and 10^4 md. We study the case where the fracture aperture is $a = 10^{-3}$. The largest difference between CVD-MPFA and the equidimensional model has been reported for this case in two previous stud-

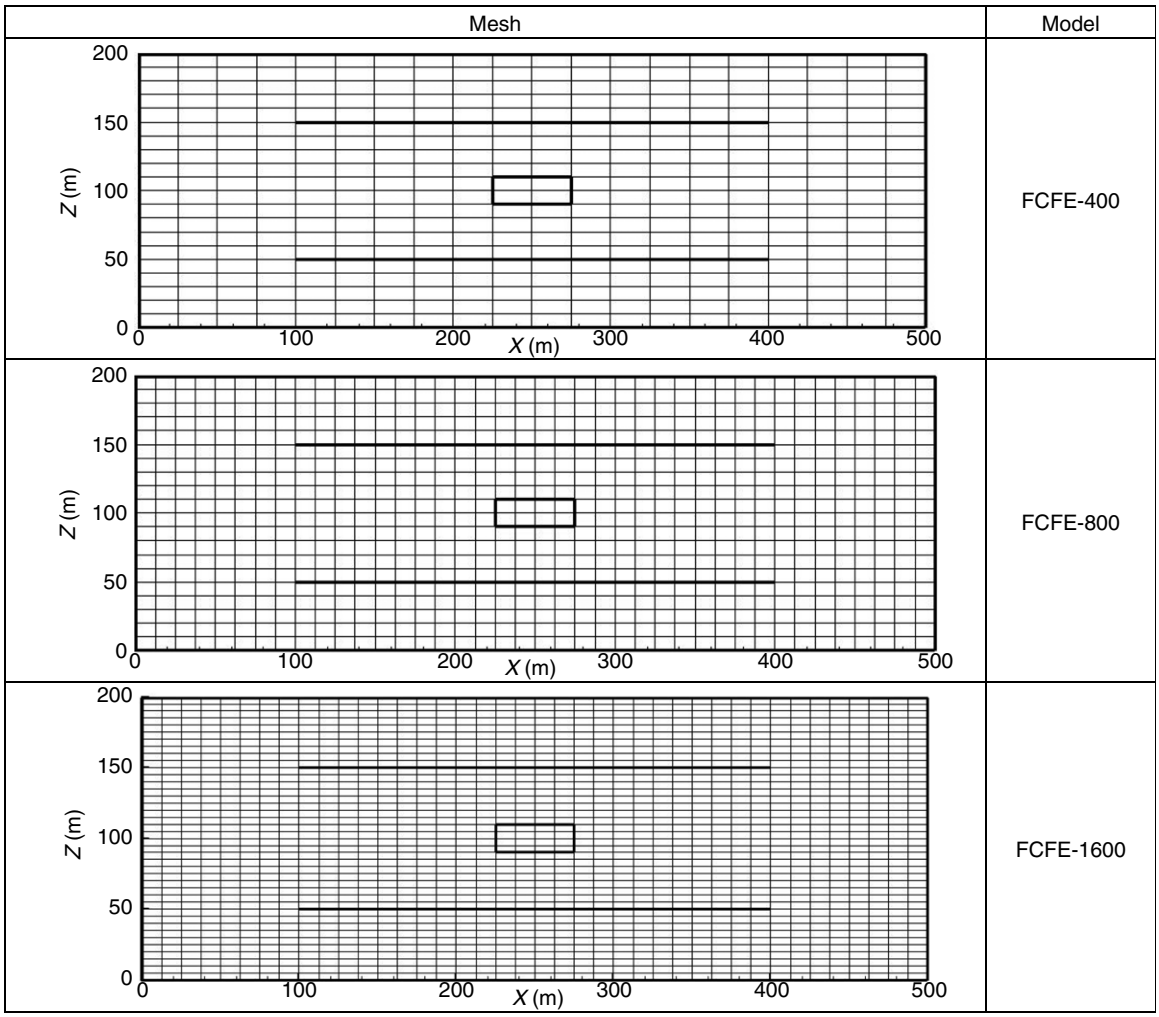

Fig. B-2—Mesh refinements in the FCFE model: Example B-1.

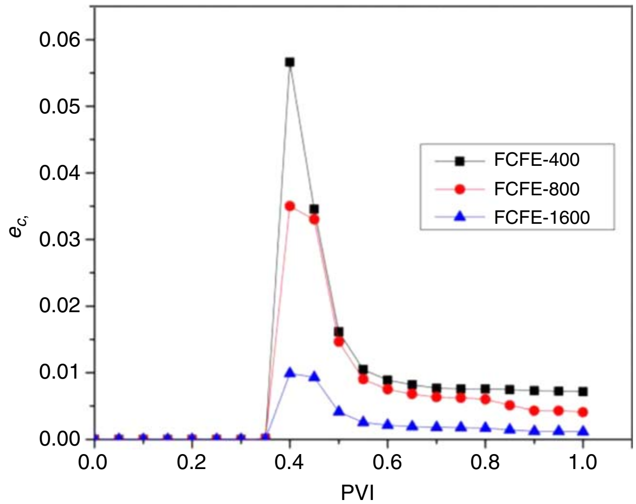

Fig. B-3—Normalized error of methane overall mole fraction at the production wells: Example B-1.

ies (Sandve et al. 2012; Ahmed et al. 2015). We use mesh refinements varying from 10×10 to 100×100 elements. The normalized error norms of pressure in our model are compared with three different numerical methods: the equidimensional method; the hybrid CVD-MPFA, which we will call CVD-MPFA-H; and the lower-dimensional CVD-MPFA, which we will call CVD-MPFA-L. The exact solution of the pressure for the incompressible single-phase flow is given by (Hægland et al. 2009):

$$p(x,y) = \begin{cases} k\cos(x)\cosh(y) + (1-k)\cos(x)\cosh(a/2), & (x,y) \in \Omega_m \\ \cos(x)\cosh(y), & (x,y) \in \Omega_f \end{cases}, \qquad \text{(B-1)}$$

for the source

$$F(x,y) = \begin{cases} (1-k)\cos(x)\cosh(a/2), & (x,y) \in \Omega_m \\ 0, & (x,y) \in \Omega_f \end{cases}, \qquad \text{(B-2)}$$

where k is the fracture/matrix-permeability ratio and Ω_m and Ω_f represent the matrix and fracture domains, respectively. In our model, Eq. 10 should be reduced to incompressible single-phase flow. **Fig. B-8** shows the convergence of the three different models. At very-low permeability, where the fracture acts as a barrier, the normalized error is the same as in the equidimensional model. Convergence plots show that similar to CVD-MPFA-H and CVD-MPFA-L, our FCFE model diverges from the equidimensional model when $k = 1$. In the high fracture permeability ($k = 10^4$), the difference becomes very small, consistent with Sandve et al. (2012) and Ahmed et al. (2015). We have examined fracture

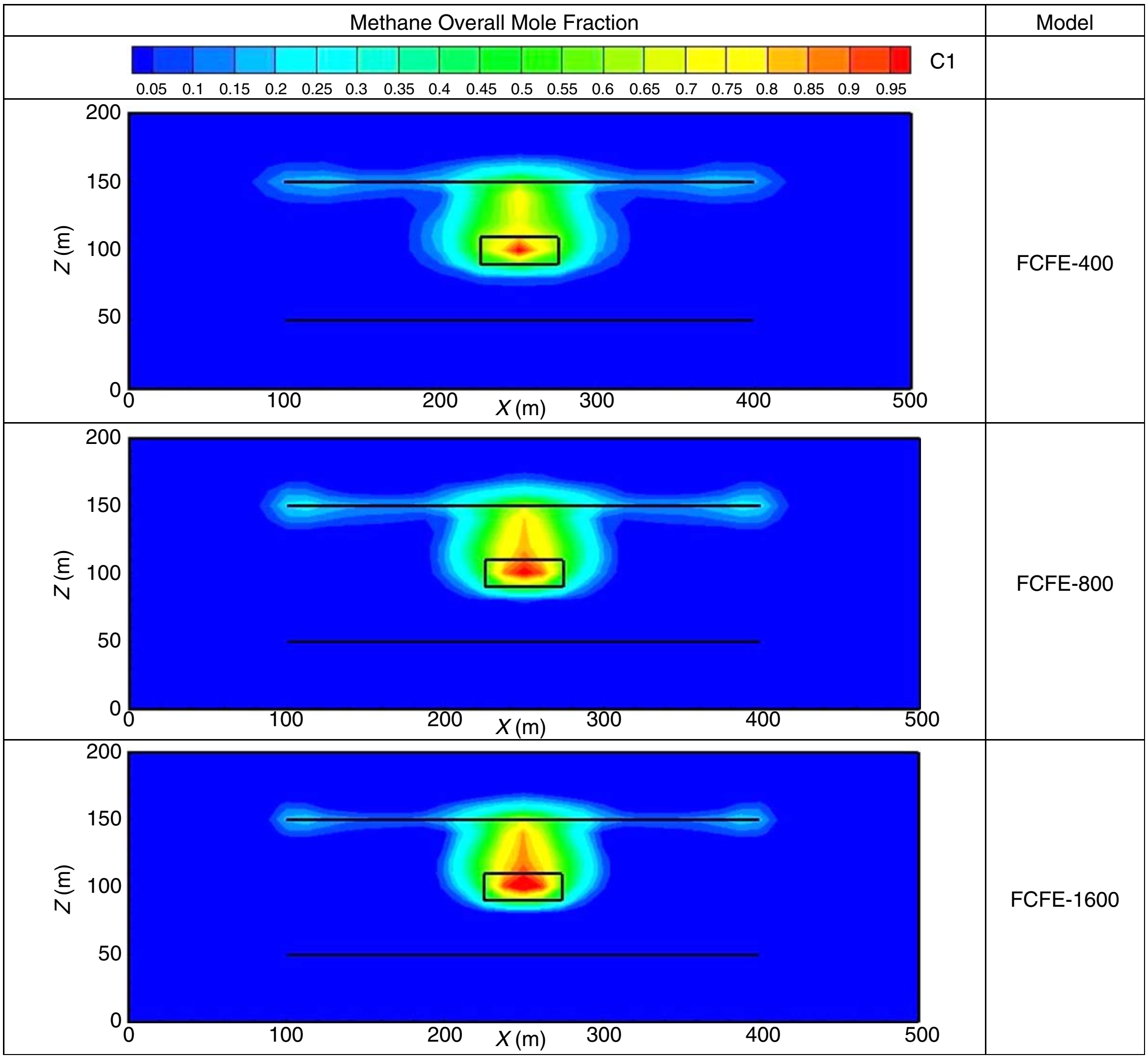

Fig. B-4—Methane overall mole fraction at 10% PVI: Example B-1.

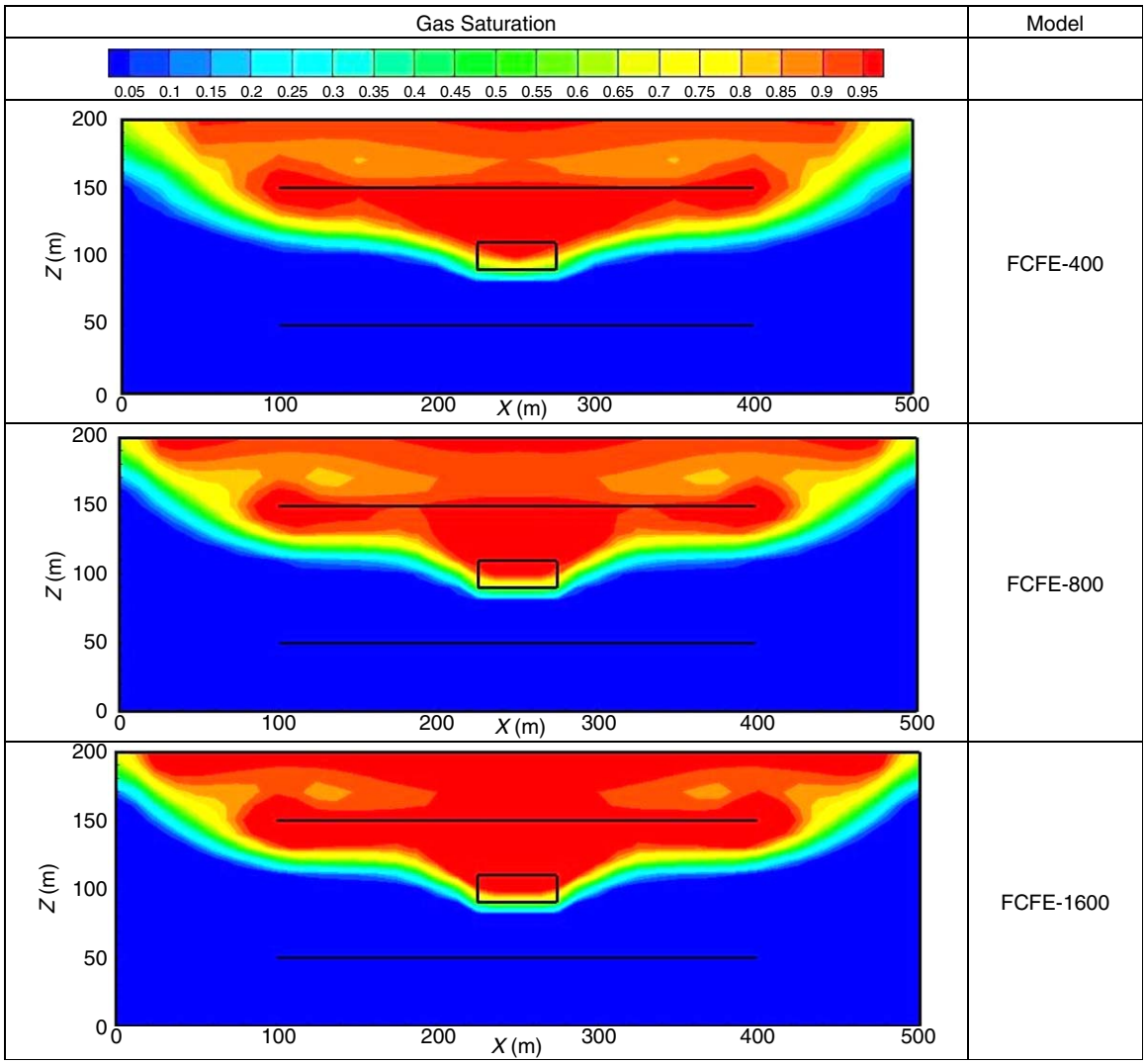

Fig. B-5—Gas saturation at 80% PVI: Example B-1.

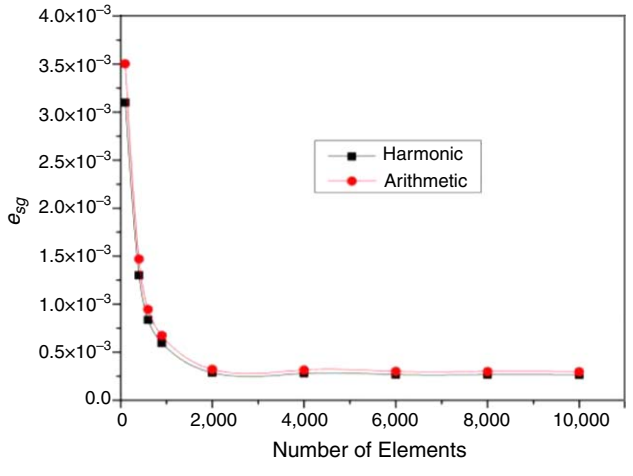

Fig. B-6—Normalized error of gas saturation in a selected matrix element: Example B-1.

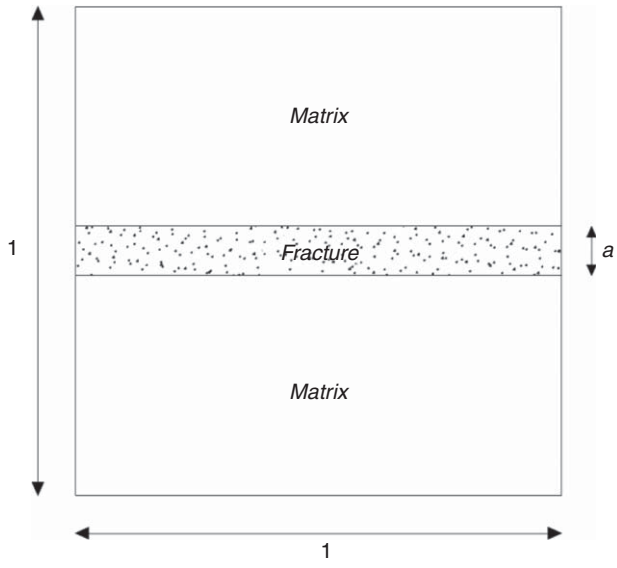

Fig. B-7—Domain with single fracture: Example B-2.

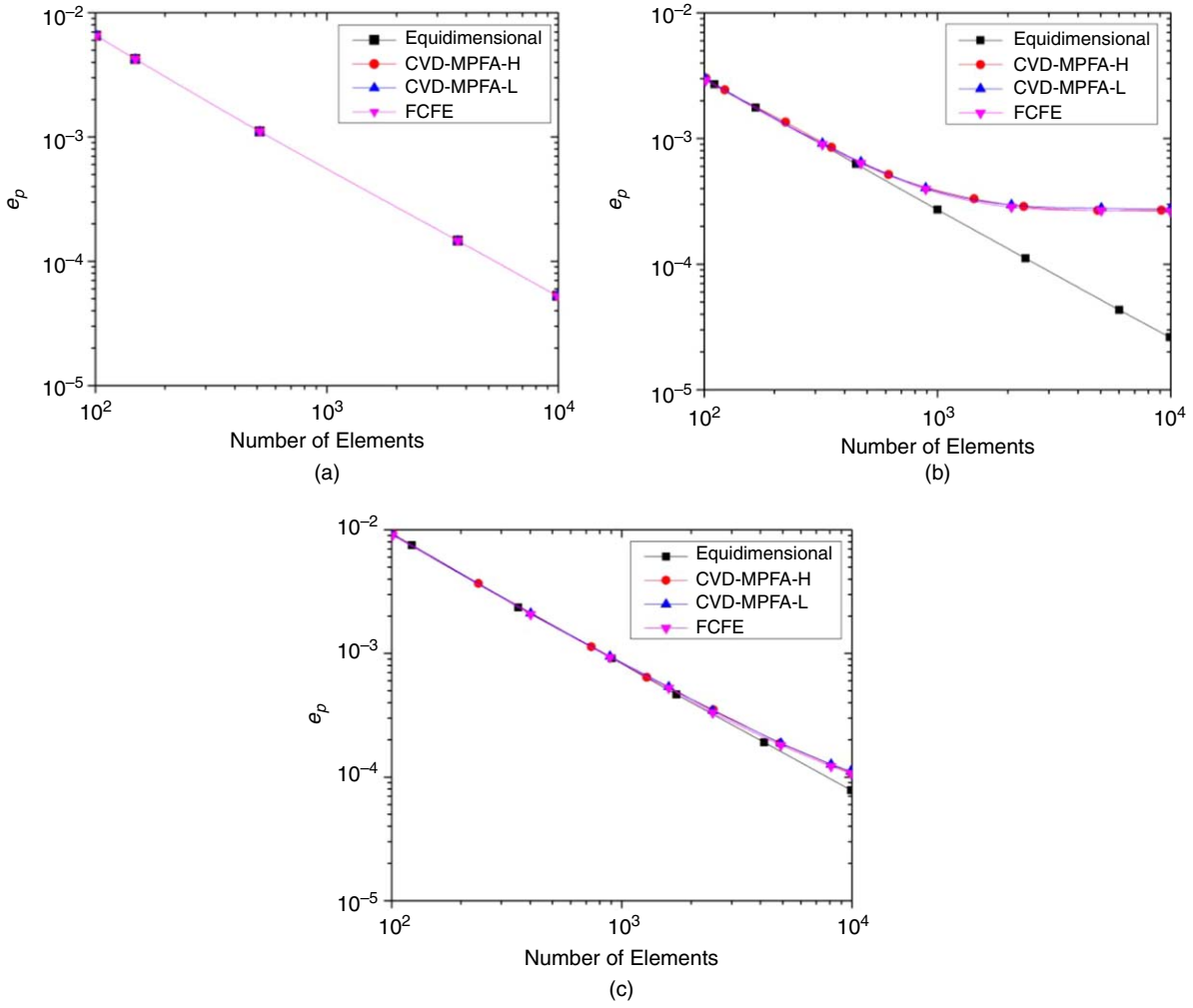

Fig. B-8—Normalized error of pressure vs. mesh refinement for different fracture permeabilities for Example B-2: (a) $k_f = 10^{-4}$, (b) $k_f = 1$, and (c) $k_f = 10^4$ md.

aperture of $a = 10^{-4}$ and 10^{-5} (results not shown) for the case of a low-permeability fracture, and the FCFE converges in all cases.

Ali Zidane is a researcher at the Reservoir Engineering Research Institute. His research interests are in the theory and advanced numerical modeling of miscible and immiscible multiphase flow in homogeneous and fractured media. Zidane holds a PhD degree in Earth sciences from Basel University, Switzerland.

Abbas Firoozabadi is the Director of the Reservoir Engineering Research Institute and a faculty member at Yale University. Recently, he was a distinguished visiting professor at Rice University in spring 2016. Firoozabadi's main research interests are in higher-order reservoir simulation of complex subsurface formations in relation to fluid injection and CO_2 sequestration; molecular structure in bulk phase; and fluid/fluid and fluid/solid interfaces in relation to oil and gas production and flow assurance. He is the author of the recent book *Thermodynamics and Applications in Hydrocarbon Energy Production* and has published approximately 210 journal papers. Firoozabadi's honors and awards include the SPE/AIME Anthony Lucas Gold Medal and membership in the US National Academy of Engineering. He holds a bachelor's degree from the Abadan Institute of Technology, Iran, and master's and PhD degrees from the Illinois Institute of Technology, Chicago; he also held a post-doctoral degree research position at the University of Michigan, Ann Arbor.